

Disentangling the Arcturus stream

Iryna Kushniruk and Thomas Bensby

Lund Observatory, Department of Astronomy and Theoretical Physics, Box 43, SE-221 00 Lund, Sweden
e-mail: [iryna; tbensby]@astro.lu.se

Received 8 February 2019 / Accepted 9 September 2019

ABSTRACT

Context. The Arcturus stream is an over-density of stars in velocity space and its origin has been much debated recently without any clear conclusion. The (classical) dissolved open cluster origin is essentially refuted, instead the discussions try to distinguish between an accretion, a resonant, or an external-perturbation origin for the stream. As kinematic structures are observational footprints of ongoing and past dynamical processes in disk galaxies, resolving the nature of the Arcturus stream can provide clues to the formation history of the Milky Way and its stellar populations.

Aims. We aim to characterise the kinematical and chemical properties of the Arcturus stream in order to resolve its origin.

Methods. The space velocities, angular momenta and actions for a sample of more than 5.8 million stars, composed from *Gaia* DR2, are analysed with a wavelet transform method to characterise kinematic over-densities in the Galactic disk. The kinematic characteristics of each identified group is used to select possible members of the groups from the GALAH and APOGEE spectroscopic surveys to further study and constrain their chemical properties.

Results. In the velocity and angular momentum spaces the already known Sirius, Pleiades, Hyades, Hercules, AF06, Arcturus and KFR08 streams are clearly identified. The Hercules stream appears to be a mixture of thin and thick disk stars. The Arcturus stream, as well as the AF06 and KFR08 streams, are low-velocity and low-angular momentum structures with chemical compositions similar to the thick disk. These three groups extend further from the Galactic plane compared to the Hercules stream. The detections of all the groups were spaced by approximately $20 - 30 \text{ km s}^{-1}$ in azimuthal velocity.

Conclusions. A wide spread of chemical abundances within the Arcturus stream indicates that the group is not a dissolved open cluster. Instead the Arcturus stream, together with the AF06 and KFR08 streams, are more likely to be part of a phase-space wave, that could have been caused by an ancient merger event. This conclusion is based on that the different structures are detected in steps of $20 - 30 \text{ km s}^{-1}$ in azimuthal velocity, that the kinematic and chemical features are different from what is expected for bar-originated structures, and that the lower-velocity streams extend further from the disk than bar-originated structures.

Key words. stars: kinematics and dynamics – galaxy: formation – galaxy: evolution – galaxy: kinematics and dynamics

1. Introduction

How large spiral galaxies form and evolve into the complicated structures that are observed today is an active area of research, and presents many challenges, both theoretically and observationally. As the Milky Way is the only galaxy where stars and structures can be studied in great detail, it may serve as a benchmark galaxy when constraining models of galaxy formation. It is therefore utterly important to understand what the Milky Way looks like, and where the observed stellar populations and structures come from. Currently the Milky Way contains a plethora of structures, both physical and kinematic, whose nature and origins are unclear.

Many studies have shown that the velocity distribution of stars in the Milky Way disk is clumpy (e.g. Dehnen 1998; Skuljan et al. 1999; Famaey et al. 2005; Antoja et al. 2008, 2012; Kushniruk et al. 2017; Ramos et al. 2018). The kinematic and chemical properties of such structures can be used to constrain the properties and the formation history of the Milky Way. For example, the Hercules stream has been widely used to probe the pattern speed and the length of the Galactic bar (e.g. Dehnen 2000; Minchev et al. 2007; Antoja et al. 2014; Wegg et al. 2015; Pérez-Villegas et al. 2017). Kinematic structures can be used to study the spiral structure of the Milky Way (e.g. Chakrabarty 2007; Sellwood et al. 2019; Quillen et al. 2018). The studies of kinematic streams especially in the Galactic halo can tell us

about the merger history of the Milky Way (e.g. Navarro et al. 2004; Helmi et al. 2006, 2017; Koppelman et al. 2018; Helmi et al. 2018). The analysis of the *Gaia* DR2 (Gaia Collaboration et al. 2018a,b) revealed that the kinematic over-densities are a part of a much more complicated structure that is seen as arches and ridges across velocity space and as clumps in action space (Trick et al. 2019). This structure is possibly caused by spiral arms or is a result of a phase-mixing due to a past merger event (e.g. Antoja et al. 2018; Ramos et al. 2018; Quillen et al. 2018). As these studies have shown, learning more about the nature of kinematic structures can improve our understanding of the Milky Way's evolution. In this paper we will investigate the properties and origin of the Arcturus stream.

A set of about 50 stars, including the star Arcturus (α Bootis), was discovered by Eggen (1971) to have very similar V space velocity component of $V \simeq -100 \text{ km s}^{-1}$. Eggen (1971) proposed that this over-density in velocity space is composed of stars that escaped from an open cluster, and was therefore named the Arcturus *moving group*. Nowadays the hypothesis of the Arcturus over-density being a moving group is almost refuted as there is no chemical homogeneity within the group (e.g. Williams et al. 2009; Ramya et al. 2012; Bensby et al. 2014), that should be if the stars originated from the same open cluster (e.g. De Silva et al. 2007; Bovy 2016). We have therefore chosen to

adopt the ‘stream’ nomenclature when referring to this Arcturus over-density of stars in velocity space.

Two other possible origins of the Arcturus stream are now favoured and are widely discussed. The first is an accretion event scenario, where a small satellite galaxy merged with the Milky Way and caused this dynamical structure (e.g. Navarro et al. 2004; Helmi et al. 2006). The second possibility is that it has originated due to resonances with the Galactic bar or spiral arms that cause kinematic over-densities (e.g. Gardner & Flynn 2010; Monari et al. 2013). The chemical properties of the stream does not show any chemical peculiarities that should be in the case of the extra-galactic origin (e.g. Ramya et al. 2012; Bensby et al. 2014). At the same time the low angular momentum and the low velocity of the stream indicate that it could be another tidal debris sub-structure in the Galactic halo (e.g. Arifyanto & Fuchs 2006; Klement et al. 2008; Zhao et al. 2014). Despite numerous approaches to study the origin of the Arcturus stream (for example, numerical simulations, kinematic analysis or studies of elemental abundances), there is no consensus on its origin.

The aim of this paper is to characterise the nature of the Arcturus stream and constrain its origin. We start detecting and characterising the velocities of the Arcturus stream using a large stellar sample constructed from the *Gaia* DR2 catalogue (see Sect. 2). Then we search for over-densities in the velocity, angular momentum and action spaces to obtain the kinematic characteristics of the stream (see Sects. 3, 4 and 5). After that we investigate the chemical characteristics of the group using the data from the GALAH (Buder et al. 2018) and APOGEE (Holtzman et al. 2018) spectroscopic surveys (see Sect. 6). We conclude by discussing possible origins for the Arcturus stream based on the kinematic and spectroscopic findings (see Sects. 7 and 8).

2. Stellar sample

To search for the Arcturus stream a wavelet analysis was applied for a stellar sample defined by velocities, angular momentum and action components. To calculate these parameters positions on the sky, proper motions, parallaxes, radial velocities, and the corresponding uncertainties for these properties are needed.

The size of the stellar sample and the quality of the astrometric data play a key role when hunting for kinematic structures. The larger the sample of stars with available high-precision astrometric data, in the greater detail it is possible to study kinematical structures of the Galaxy. The currently best data source is the *Gaia* satellite, which is an on-going full-sky mission that aims to provide high-precision astrometric parameters for more than a billion targets over the whole sky. The most recent data release, *Gaia* DR2 (Gaia Collaboration et al. 2018a) contains astrometric data for almost 1.7 billion targets, and for a small subsample of about 7 million targets, also radial velocities.

A stellar sample of 5 844 487 stars was constructed from the *Gaia* DR2 catalogue in the following way:

- 7 173 615 stars were obtained from McMillan (2018), who estimated distances for *Gaia* DR2 stars with measured radial velocities.
- Stars with bad fits of *Gaia* DR2 astrometric parameters were filtered out to avoid possible systematic errors in the stellar sample. Following the procedure suggested in Lindegren (2018) a re-normalised unit weight error (*RUWE*) is used to estimate goodness of astrometric fits. Selecting those targets with *RUWE* < 1.4 leaves us with 6 692 285 targets. Photometric filtering that cleans the sample from star with bad

astrometric solutions (see Eq. 2 in Arenou et al. (2018)) was also applied. This cut leaves us with 6 683 408 stars.

- Space velocities U, V, W^1 together with angular momenta and actions that will be used later in this paper were computed using *galpy*² package (Bovy 2015). For action estimates we used MWPotential2014 axisymmetric gravitational potential model pre-defined in *galpy*. Velocity uncertainties $\sigma_U, \sigma_V, \sigma_W$ were computed following equations from Johnson & Soderblom (1987). The velocities are given relative to the Local Standard of Rest: $(U_\odot, V_\odot, W_\odot) = (11.1, 12.24, 7.25)$ km s⁻¹ (Schönrich et al. 2010). Taking into account the results from, for example, Zhao et al. (2014), that the typical size of kinematical structures is around 20 km s⁻¹. Therefore we need to cut stars with $\sigma_U, \sigma_V > 20$ km s⁻¹, because such large velocity uncertainties will influence the precision of the results, that is the position in velocity space of the structures. This leaves us with 6 002 514 stars.
- Next, the sample was constrained to stars that are located within a distance of 5 kpc from the Sun. This filters out stars that are located in the outskirts or very inner parts of the Galaxy, and thus, cannot be a part of any of the local kinematic structures. The limit of 5 kpc was chosen to avoid regions in direct contact with for example the Galactic bar, whose half-length is about 3 kpc (e.g. Dehnen 2000; Minchev et al. 2010; Monari et al. 2017). According to (Bailer-Jones 2015) distance estimates should not be dominated by using pre-*Gaia* information or so-called priors if fractional parallax uncertainty does not exceed 20%. Typical parallax uncertainty for bright sources in *Gaia* DR2 is about 0.4 μ as Lindegren (2018). Converting 5 kpc cut into μ as and calculating fractional parallax uncertainty we obtain 20% meaning that distance estimates in the sample should not be effected by priors. After this cut there are 5 844 487 stars left that will go into our analysis.

Since kinematic structures are local phenomena (e.g. Antoja et al. 2012; Ramos et al. 2018; Trick et al. 2019) and the stellar sample covers a wide range in X and Y , it was divided into 66 smaller volumes that were investigated separately. Each box is 0.4 kpc in radial coordinate and 3° in azimuthal angle³. The top plot in Fig. 1 shows the distribution of the 5 844 487 stars in the Galactic Cartesian $X - Y$ plane and how it is divided into small volumes. The name of each region, the number of stars, the median distance from the Sun, and median distance uncertainty are given in Table A.1 for each of the 65 volumes. The bottom plot in Fig. 1 shows the sample in Cartesian X and Z coordinates, where Z is a vertical component of Galactocentric coordinate system (points towards North Galactic Pole).

3. Method

Our current knowledge about the Arcturus stream is based on observations within a small region of about 500 pc around the Sun. Its origin is unknown, mainly due to that there are only rough estimates of its kinematic characteristics, and as it is chemical properties are not well studied. Our strategy is therefore to

¹ U points towards Galactic centre, V velocity defines the direction of the Galactic rotation, W points at the North Galactic Pole.

² Available at <http://github.com/jobovy/gaipy>

³ R is the radial coordinate pointing towards the Galactic anti-centre, and ϕ is the azimuthal angle following the direction opposite to the Galactic rotation.

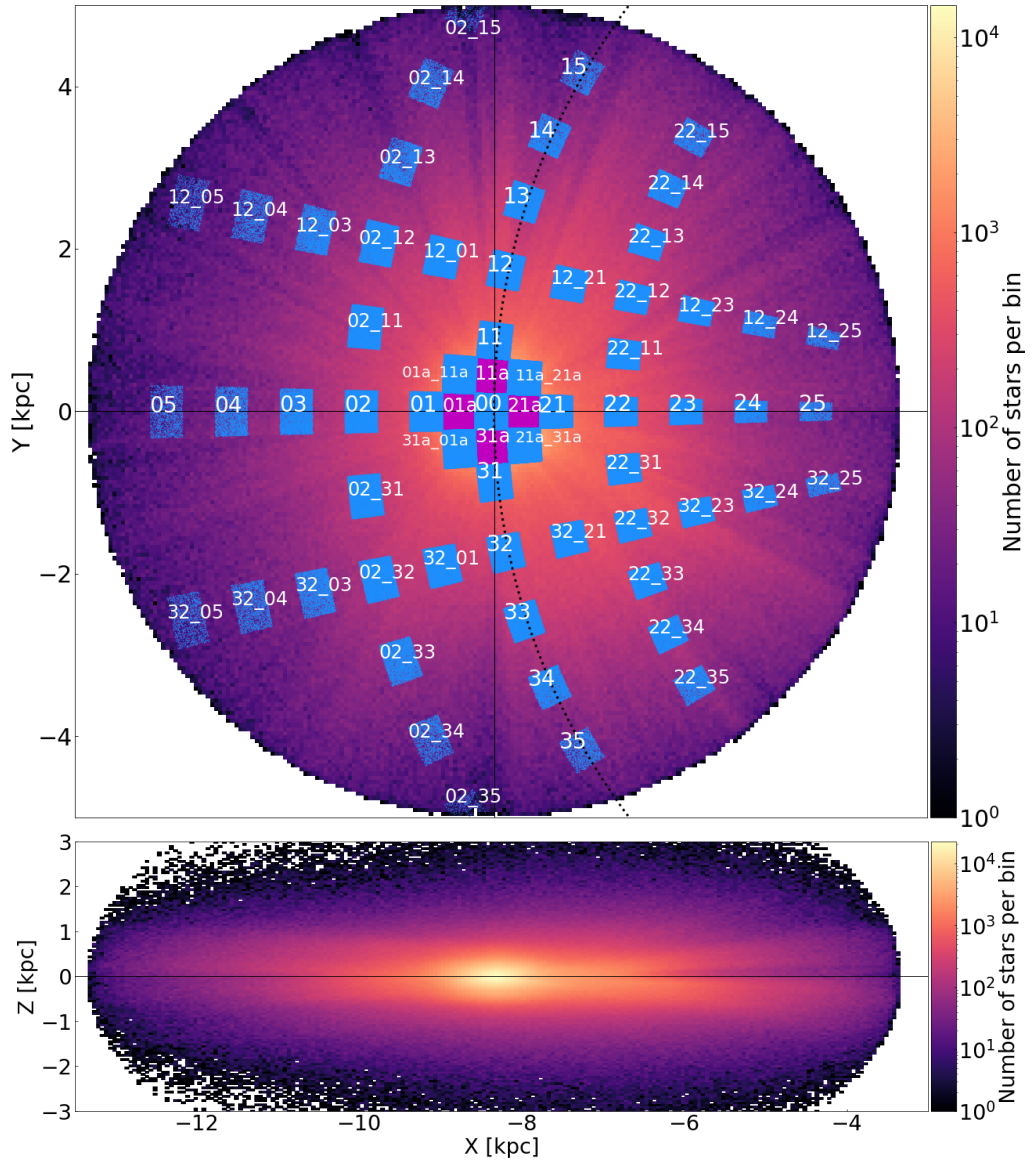


Fig. 1. Distribution of 5 844 487 stars with σ_U and $\sigma_V < 20 \text{ km s}^{-1}$ and $R \leq 5 \text{ kpc}$ in X and Y (top), and X and Z (bottom) Cartesian Galactic coordinates. Blue and magenta boxes show 66 small regions investigated in this work and their names are written on top in white color. The dashed line in the top plot shows the Solar circle. The black line in the bottom plot shows $Z = 0 \text{ kpc}$. The bin size is 0.05 kpc for both plots.

search for streams in four different planes defined by combinations of velocity, angular momentum and action components respectively: the $U - V$ plane, the $V - \sqrt{U^2 + 2V^2}$ plane, the $L_z - \sqrt{L_x^2 + L_y^2}$ plane, and the $L_z - \sqrt{J_r}$ plane. This will allow us to characterise structures in terms of velocities, angular momenta and actions, and obtain stronger criteria on how to select stars-members of kinematic structures.

3.1. Investigated planes

The distributions of stars in all four planes are shown Fig. 2. A majority of stars have negative V velocities between $V \approx 0$ and -200 km s^{-1} and angular momentum L_z between 0 and $2500 \text{ kpc km s}^{-1}$. The disk stars are located at $L_z \approx 1800 \text{ kpc km s}^{-1}$, the halo stars are expected at $L_z \approx 0 \text{ kpc km s}^{-1}$.

3.1.1. The $U - V$ plane

The $U - V$ plane is widely used to search for kinematic structures (e.g. Dehnen 1998; Antoja et al. 2008, 2012; Kushniruk et al. 2017; Antoja et al. 2018; Ramos et al. 2018; Katz et al. 2019). It allows to trace kinematic over-densities of different origin without making any assumptions on orbital parameters of stars as well as no assumptions on the Galactic potential. The only limitation of this method is that stellar volumes must be relatively small (around $0.1 - 0.5 \text{ pc}$ in X and Y , see Trick et al. 2019), since kinematic structures in the $U - V$ plane are local. On the other hand, this limitation is an advantage, since it allows us to follow how the structures move in physical space (Ramos et al. 2018). The Arcturus stream is expected to be one of the arches in the $U - V$ plane localised around $V \approx -100 \text{ km s}^{-1}$ in the nearby sample. The stream is likely to cover a wide range of U velocities (Williams et al. 2009).

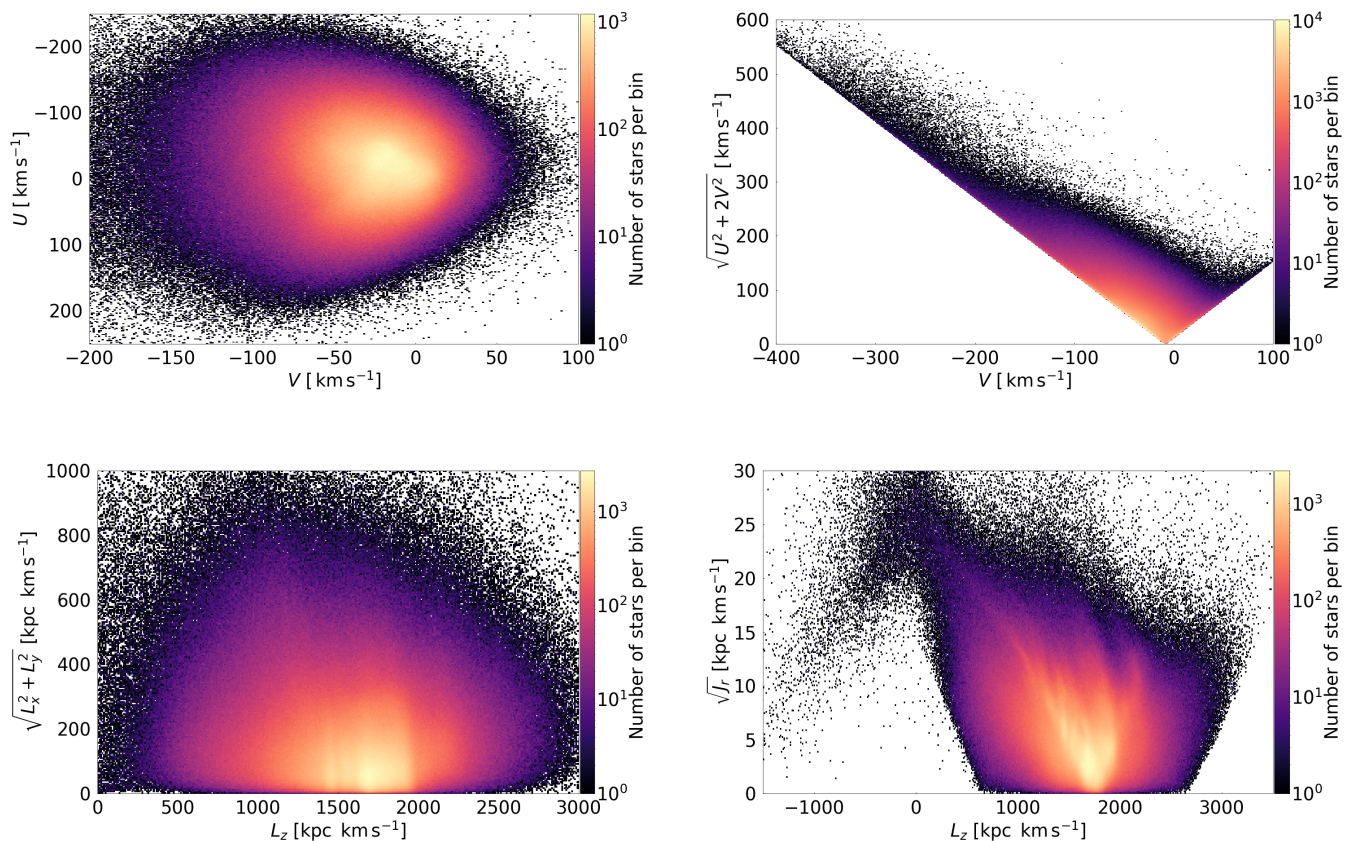


Fig. 2. Density map of the selected sample of 5 844 487 stars in $U - V$ space (top left), in $V - \sqrt{U^2 + 2V^2}$ space (top right), in $L_z - \sqrt{L_x^2 + L_y^2}$ space (bottom left) and in $L_z - \sqrt{J_r}$ space (bottom right). The bin sizes are 1 km s^{-1} , 1 km s^{-1} , 10 kpc km s^{-1} and $10 \times 0.1 \text{ kpc km s}^{-1}$, respectively.

3.1.2. The $V - \sqrt{U^2 + 2V^2}$ plane

Examining the distribution of stars in the $V - \sqrt{U^2 + 2V^2}$ plane was proposed by Arifyanto & Fuchs (2006). V is proportional to L_z , a vertical component of the angular momentum and is an integral of motion in axisymmetric potentials. $\sqrt{U^2 + 2V^2}$ is a measure of eccentricity in the Dekker's approximation (Dekker 1976). This means that we search for structures that share similar orbital eccentricity. This approach is applicable only for planar orbits in axisymmetric potentials. The method shows reliable results for nearby stars with eccentricities up to 0.5 (Arifyanto & Fuchs 2006). The $V - \sqrt{U^2 + 2V^2}$ plane was used by Klement et al. (2008) and Zhao et al. (2014) to search for kinematic structures and allowed to reveal several structures including the Arcturus stream. We expect to detect the Arcturus stream at the velocities around $V - 100 \text{ km s}^{-1}$ in the solar neighbourhood (e.g. Williams et al. 2009).

3.1.3. The $L_z - \sqrt{L_x^2 + L_y^2}$ plane

Another approach to search for kinematic groups was proposed by Helmi et al. (1999) who suggested to examine distribution of stars in the plane characterised by the L_z and $\sqrt{L_x^2 + L_y^2}$ integrals of motion, where L_x , L_y , and L_z are angular momentum components in X , Y and Z directions. The method is used to search for phase-mixed stars on similar orbits. The disadvantage of this

method is that $\sqrt{L_x^2 + L_y^2}$ is not fully conserved in axisymmetric potentials, but still allows to reveal dynamical structures (e.g. Helmi et al. 1999; Klement et al. 2008; Zhao et al. 2014). The Arcturus stream is expected at L_z in the range between 700 and 1100 km s^{-1} kpc (e.g. Navarro et al. 2004).

3.1.4. The $L_z - \sqrt{J_r}$ plane

The most general method to search for kinematic structures is to investigate action space. Actions are conserved quantities that characterise stellar orbits. In this work we will use radial and azimuthal actions J_r and L_z that are a measure of orbital eccentricity and orbital angular momentum. As suggested in Trick et al. (2019) taking the square root of radial action will make the final plots more clear. The action space was investigated by, for instance, Sellwood (2010) and Trick et al. (2019) and is rich on kinematic over-densities as. We expect to detect the Arcturus stream at L_z in the range between 700 and 1100 kpc km s^{-1} (e.g. Navarro et al. 2004).

3.2. Wavelet transform

To search for kinematic structures the methodology described in Kushniruk et al. (2017) was used with some additions. To detect over-densities a wavelet transform was applied to the stellar sample in the $U - V$, $V - \sqrt{U^2 + 2V^2}$, $L_z - \sqrt{L_x^2 + L_y^2}$, and $L_z - \sqrt{J_r}$ planes. Then the noise from the wavelet maps was fil-

tered and Monte Carlo simulations were used to verify whether the detected structures are real or not.

The data was analysed by the wavelet transform with the ‘*atrous*’ algorithm (Starck et al. 1998) applied to the stars in all 65 regions in the four different planes separately. The input data is a binned stellar density map in the velocity, angular momentum and action planes. The bin sizes Δ were set to 1 km s^{-1} for the $U - V$, and the $V - \sqrt{U^2 + 2V^2}$ planes, to 2 km s^{-1} kpc for the $\sqrt{L_x^2 + L_y^2} - L_z$ plane, and to $0.1 \times 10 \text{ kpc km s}^{-1}$ for the $L_z - \sqrt{J_r}$ plane. Due to the limitations of the usage of the $V - \sqrt{U^2 + 2V^2}$ plane, as discussed in Sect. 3.1.2, the stars that have orbits with eccentricities $e > 0.5$ were cut out. The output data is a set of wavelet coefficients at different scales that contain information about the presence of substructures. A higher wavelet coefficient means a higher probability that the structure is real. The scale J is proportional to the size of the detectable structures s . Scales $J = 1, 2, 3$ and 4 were investigated for all maps. The relation between scale and bin size $s_J = 2^J \Delta$ characterises typical sizes of detectable structures. Then the wavelet coefficient maps were filtered from Poisson noise. The wavelet transform part as well as noise filtering from the output wavelet maps were performed in MR software⁴ developed by CEA (Saclay, France) and Nice Observatory. More details on the algorithm itself can be found in Starck & Murtagh (2002), and more details on the methods used to search for overdensities and structures can be found in Kushniruk et al. (2017).

3.3. Acquiring positions of the detected peaks

To get precise positions of the peaks Monte Carlo (MC) simulations were performed. MC samples were created assuming that each star can be represented as a Gaussian velocity distribution with $\mu = (U, V)$ and $\sigma = (\sigma_U, \sigma_V)$ for the two velocity components. To generate MC samples in angular momentum and action space orbits of stars were computed assuming that positions, proper motions and radial velocities can be represented as Gaussians, similarly as velocities. Here it is assumed that Gaussians are independent and do not consider correlations between astrometric parameters. These MC samples are then analysed in the same manner as the original data. Convergence is reached when the number of structures and their positions do not change as more simulations are added. Typically, results converge after about 30 simulations, but to be on the safe side, 100 MC samples were created for all regions. Then MC wavelet maps for different scales were over-plotted used to search for peaks applying *peak_local_max* feature from *scikit-image*⁵ Python package (van der Walt et al. 2014). In this work we focus on the $J = 2$ and $J = 3$ scales as they allow us to detect most structures.

4. Results

4.1. Stellar streams in the nearby sample

Figures 3 and 4 show 100 over-plotted wavelet maps for the central region 00 in four different planes for scales 2 and 3, respectively. Both scales show richness of kinematic structures for the nearby sample. The list of the centres of the peaks and the corresponding uncertainties are given in Table A.2 for scale $J = 2$ and in Table A.3 for scale $J = 3$. The fact that well-known

groups like Sirius, Coma Berenices, Hyades, Pleiades and Hercules were identified at the expected positions shows that our method is sound (see Tables 3, 5, 6 and 7 in Kushniruk et al. 2017 that summarise literature values for the U and V velocities of Sirius, Coma Berenices, Hyades, Pleiades and Hercules). These groups are detected in all four planes. The detection of other groups varies between the planes. Figure 3 for scale $J = 2$ shows the same structures as in Fig. 4 for scale $J = 3$ but in greater details. It was decided to focus on scale $J = 2$ since it is more sensitive to smaller structures. By comparing our results in the nearby region ‘00’ (centred around the Sun, see Fig. 2) for scale $J = 2$ with what has previously been found in the literature (e.g. Eggen 1998; Navarro et al. 2004; Arifyanto & Fuchs 2006; Klement et al. 2008; Williams et al. 2009; Antoja et al. 2012; Zhao et al. 2014; Kushniruk et al. 2017; Trick et al. 2019; Antoja et al. 2018; Ramos et al. 2018)) we assign names to the structures. Curved lines and boxes of different colours in Figs. 3 and 4 correspond to the names of the groups listed in the legend of Fig. 3. The structures found in the nearby region are discussed below:

- **A1/A2:** Groups with $V > 15 \text{ km s}^{-1}$ and $L_z > 2000 \text{ kpc km s}^{-1}$ we link to arches A1 and A2 detected by Ramos et al. (2018) (see their Table 2). A1/A2 is shown with yellow lines and boxes on the plots.
- **Sirius:** Blue line and boxes correspond to the Sirius stream. Group 13 in the $U - V$ space is potentially Bobylev16 (see Bobylev & Bajkova 2016) and could be a continuation of Sirius.
- **γ Leo:** Pink line slightly above Sirius in V is γ Leo stream (see Antoja et al. 2012). Unlike a big majority of the groups, γ Leo is located at positive U velocities. The stream could be a continuation of Sirius arch since both have similar angular momenta.
- **Coma Berenices:** Magenta line just below Sirius is Coma Berenices stream. Unlike arch-like neighbouring Sirius and Pleiades/Hyades, Coma Berenices is a clump in the $U - V$ plane and, consequently, is a shorter line in the angular momentum space.
- **Dehnen98/Wolf630:** Wolf630 and Dehnen98 (see Antoja et al. 2012; Dehnen 1998) are two small groups in between Coma Berenices and Pleiades/Hyades streams. They are shown with brown colour and could be a continuation of Coma Berenices.
- **Pleiades/Hyades:** A grey arch in the $U - V$ plane is associated with Pleiades/Hyades stream. Group 29 in the $U - V$ space linked to Antoja12(15) (see Antoja et al. 2012) could be a continuation of stream.
- **Hercules:** Orange lines and boxes correspond to the Hercules stream. It is likely to be composed of a few substructures that are visible in the angular momenta and action spaces.
- **HR1614:** The HR1614 moving group (see Feltzing & Holmberg 2000; De Silva et al. 2007) we connect to the clumps just below Hercules in V . The group is shown with a lime colour.
- **ϵ Ind:** Groups g34 and g35 in the $U - V$ plane are linked to a group called ϵ Ind (see Antoja et al. 2012). The structure is marked with a black colour.
- **AF06:** AF06 stream was first found by Arifyanto & Fuchs (2006) in the range between $V \simeq -70$ and -100 km s^{-1} . We did not find it in the $U - V$ space, but the group is detected in other three spaces and is shown with red boxes.

⁴ Available at <http://www.multiresolutions.com/mr/>

⁵ <https://scikit-image.org/>

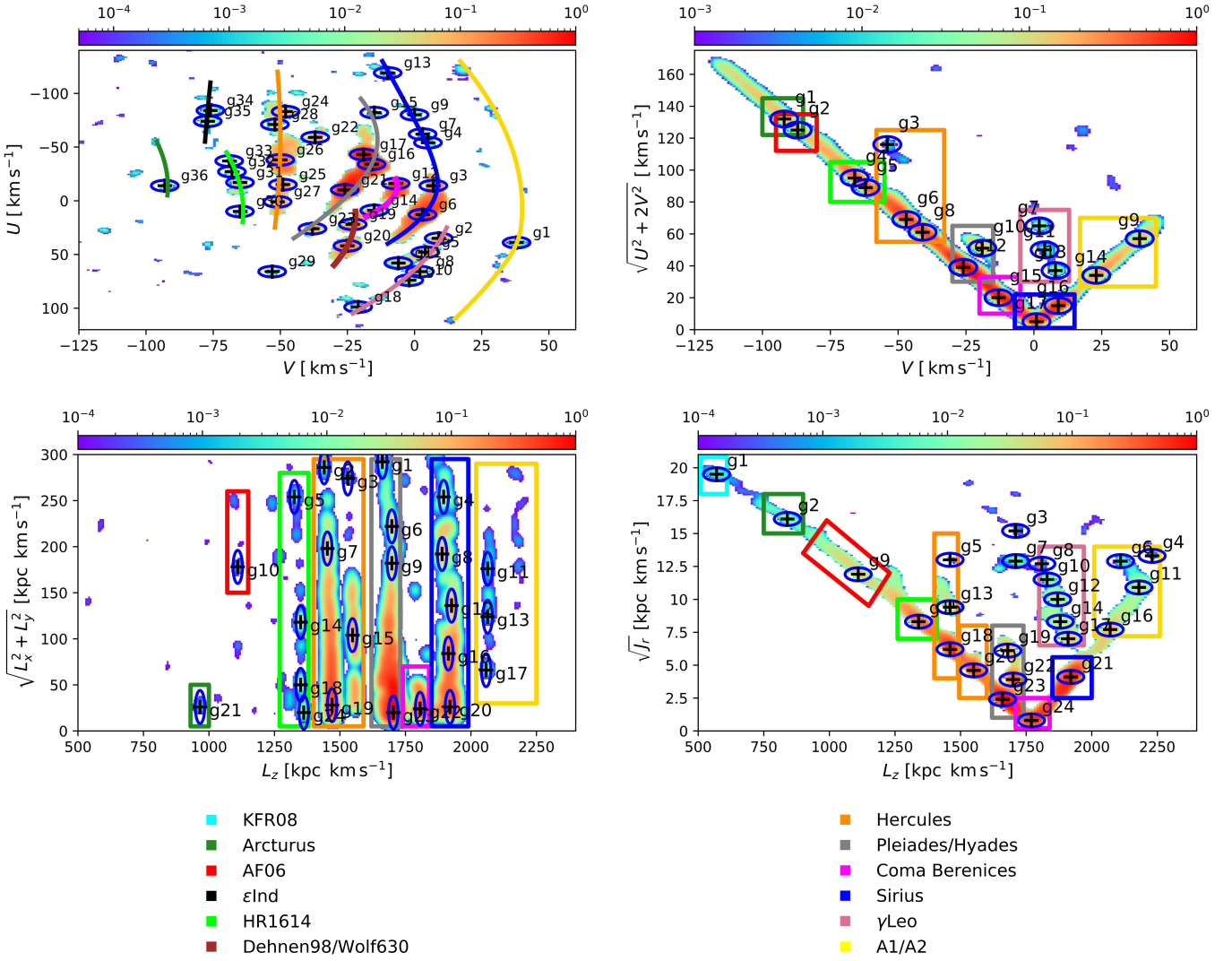


Fig. 3. Wavelet coefficient maps of central region 00 retrieved in $U - V$ (top left), $V - \sqrt{U^2 + 2V^2}$ (top right), $L_z - \sqrt{L_x^2 + L_y^2}$ (bottom left) and $L_z - \sqrt{J_r}$ (bottom right) space for scale $J = 2$. Colour bars show normalised wavelet coefficients. Kinematic structures are shown as blue circles with radius 5 km s^{-1} or 5 kpc km s^{-1} and their centres are shown with black crosses. Lines and boxes of different colours correspond to the group names as listed in the legend. Note that numbers assigned to the groups do not match between the planes.

- **Arcturus:** Group g36 in the $U - V$ plane could be the Arcturus stream. Median V velocity and angular momentum of g36 are $V \approx -92 \text{ km s}^{-1}$ and $L_z \sim 1118 \text{ kpc km s}^{-1}$. These values are a bit higher compared to, for example, values from Navarro et al. (2004), but are within the uncertainties. In the $V - \sqrt{U^2 + 2V^2}$ plane the nearest to Arcturus are groups g1 and g2 and have the same angular momentum and radial action as g36 in the $U - V$ plane. In the angular momentum space g21 has the parameters closest to Arcturus. In action space there are two candidates: g9 and g2. The first group is consistent with the groups detected in velocity spaces, the second one has lower angular momentum and V velocity. Taking into account works by Klement et al. (e.g. 2008); Zhao et al. (e.g. 2014) we link g2 to the Arcturus stream and group g9 to the AF06 stream. Arcturus is shown as green lines and boxes on the wavelet maps.
- **KFR08:** Among the detected groups we assign one weak over-density in action space at $L_z \approx 575 \text{ kpc km s}^{-1}$ to the group called KFR08. The structure was first detected by Klement et al. (2008) at $V \approx -160 \text{ kpc km s}^{-1}$. Group g1 in de-

tected in action space has exactly the same median V velocity. KFR08 is shown with cyan colour on the wavelet maps.

Overall 36 groups at scale $J = 2$ and 16 groups at scale $J = 3$ were discovered in the $U - V$ plane that form larger-scale arches as discussed in Ramos et al. (2018); Antoja et al. (2018); Gaia Collaboration et al. (2018b). We also conclude that these arches correspond to the lines in the $L_z - \sqrt{L_x^2 + L_y^2}$ plane and to clumps in the $V - \sqrt{U^2 + 2V^2}$ and $L_z - \sqrt{J_r}$ due to very similar properties of the groups (see Tables A.2 and A.3). In the $V - \sqrt{U^2 + 2V^2}$ 17 and 8 groups were detected respectively. Action space mimics $V - \sqrt{U^2 + 2V^2}$ plane very much but allows to detect the structures in greater detail. In the angular momentum and action spaces 24 groups were found in each space at scale $J = 2$ and 9 and 10 groups at scale $J = 3$, respectively.

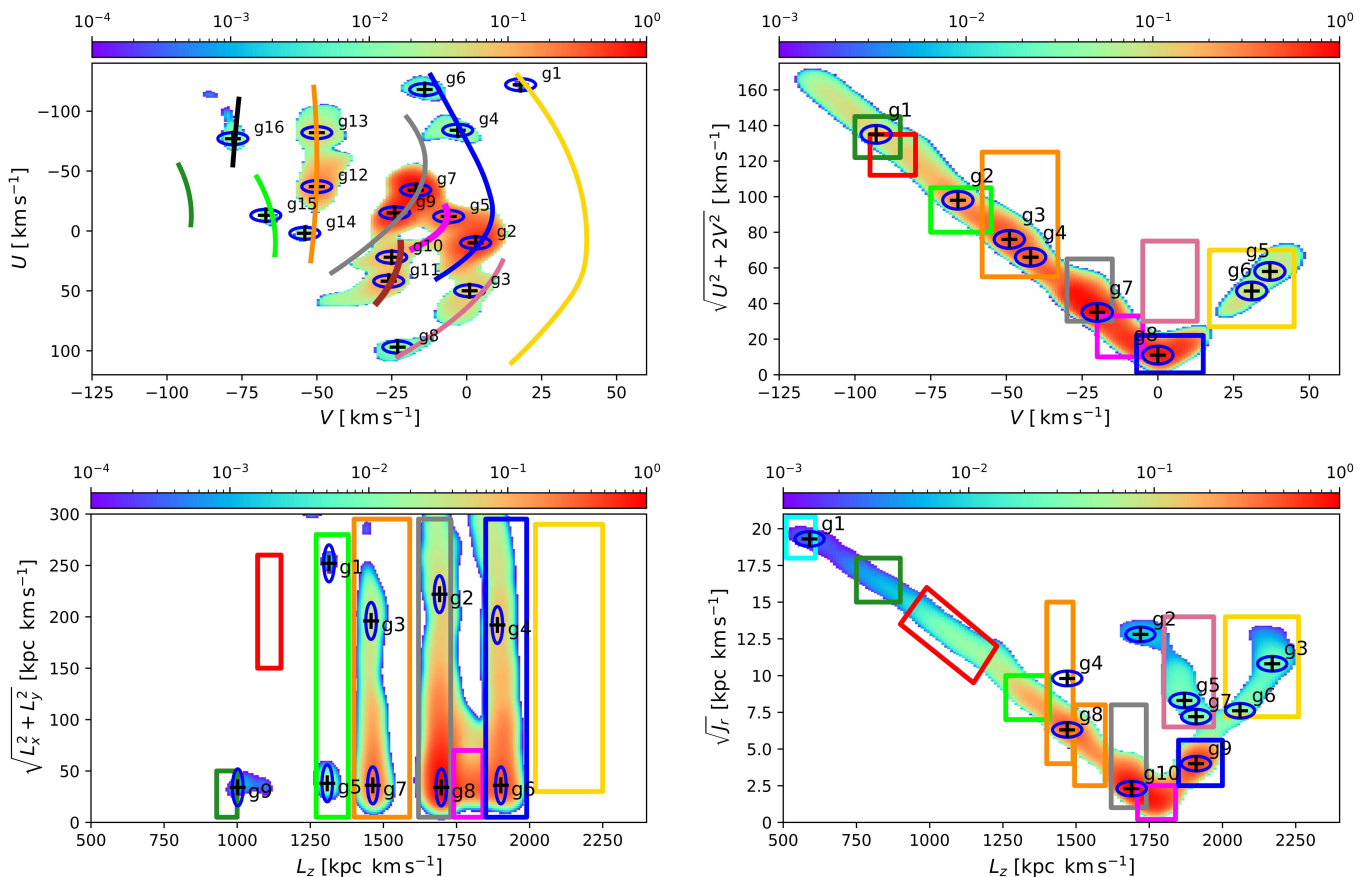


Fig. 4. Same as Figure 3 but for scale $J = 3$. Lines and boxes correspond to the structures detected at scale $J = 2$. Note that numbers assigned to the groups do not match between the planes.

4.2. Stellar streams outside the solar neighbourhood

The solar neighbourhood volume is well-studied and thus it is relatively easy to match the detected groups with groups that have been identified by other studies in the literature. The behaviour of the groups outside the solar volume was studied by (Antoja et al. 2012; Ramos et al. 2018, e.g.). Both papers found a decreasing trend for V velocity when moving to the volumes at larger R . In this work we also investigated the trends of the structures depending on the position in the Galaxy with a focus on the Arcturus stream.

If one looks at the small volumes from the left-hand side of Fig. 2 and move towards positive X values an increase in V velocity can be observed. As an example of this trend Fig. 5 shows how the V velocity of the groups evolves with Galactocentric distance R in regions 01, 01a, 00, 21 and 21a based on the analysis of the $U - V$ plane. For example, the Hercules stream in region 01 is detected at $V \simeq -70 \text{ km s}^{-1}$, and for comparison, in region 21a the Hercules stream shifts towards positive V and is located at $V \simeq -40 \text{ km s}^{-1}$. Similar behaviours is observed for most of the major streams and is shown in the top plot of Fig. 5. On the wavelet maps for regions 01a and 21a that are shown in the middle and bottom plots of Fig. 5 we draw the lines from the top left plot in Figure 3. Taking volumes at larger R shifts the groups towards lower V values and vice versa.

If one fixes the galactocentric distance and starts exploring the regions at high ϕ moving down towards negative ϕ (for example, start at region 15 and go down to region 35), the streams are observed at the same position in V . Major streams includ-

ing Sirius, Pleiades, Hyades and Hercules have the same angular momentum when fixing R and looking at different ϕ . This is different from results in Monari et al. (2019) who found that the Hercules angular momentum changes with azimuth at solar radius. We also do not observe this change when fixing R inside and outside the Solar circle.

The shape of the angular momentum and action spaces change a bit at different R , but almost all main structures detected in the solar volume remain at the same positions within a box defined by volumes 02_12, 22_12, 22_32 and 02_32. Figure 6 shows wavelet transform maps for regions 01a and 21a (top and middle rows). Additionally a wavelet transform was applied to all the stars in the sample in the angular momentum and action spaces (bottom row) and compare to results in volumes 01a and 21a. If there are any groups with constant actions detected in the total sample then it possible to observe them in smaller volumes. Boxes of different colours mark kinematic structures detected in the region 00. The same boxes are plotted on top of maps for regions 01a and 21a. There is a small shift in action space when changing R , but generally main groups are located at the same positions.

The kinematic structures are mainly detected in the central regions within the rectangle defined by regions 02_12, 22_12, 22_32 and 02_32. The rest of the regions contain less stars and also have larger distance uncertainties. We tested if the structures really exist only inside the mentioned above box or the lack of the groups in the outer regions is a consequence of larger distances and smaller number of stars in sub-samples. To check if the latest is true 10 000 stars were randomly selected in the

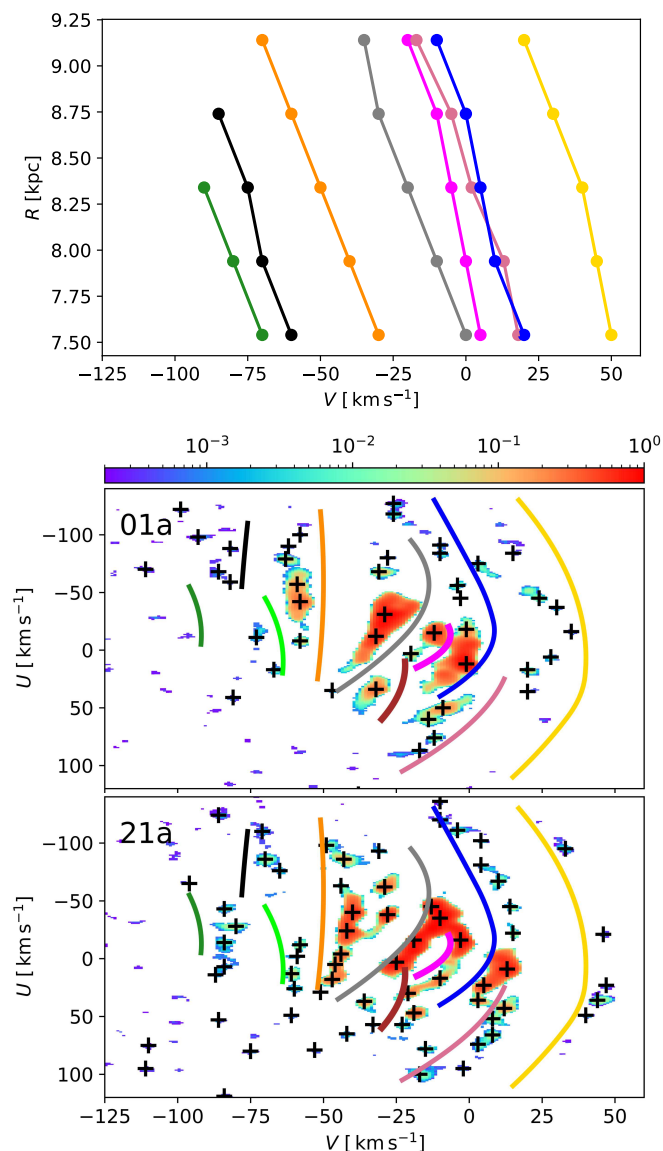


Fig. 5. *Top plot:* Change of central V velocities of kinematic structures as a function of Galactocentric radii R . Each dot corresponds to the centre of the structure determined by the wavelet transform in volumes 01, 01a, 00, 21 and 21a. Names of the groups associated with the lines are listed in the legend of Figure 3. *Middle and bottom plots:* Example of wavelet maps in the $U - V$ space in regions 01a and 21a. Colour bar shows normalised wavelet coefficients. Black crosses show centres of the detected structures in regions 01a and 21a. Lines show the location of kinematic structures detected in region 00 (see legend of Fig. 3).

central region 00 and repeated the wavelet analysis. Then, the results were compared with Dehnen (1998) who used a sample of 14 000 stars in total. For our 10 000 sample a similar result as Dehnen (1998) was received. The main conclusion of the test is that with the small samples it is possible to detect only main big structures like Sirius, Hyades, Pleiades and Hercules. The more stars are in the volume, the higher is the probability to detect low-velocity structures. Due to this limitation, it is not possible claim that there is such a radius where some of the groups stop existing.

There are many tiny groups detected in the $U - V$ plane that could potentially be a part of the Arcturus stream. We do not observe a clear arch that we can connect with the structure. Un-

like the Arcturus stream, an arch at $V \approx -80 \text{ km s}^{-1}$ is clearly visible inside a box defined by regions 01, 11, 21, 31 for the AF06 stream. In the $V - \sqrt{U^2 + 2V^2}$ plane the structures are better resolved at scale $J = 3$. In the angular momentum and action space there are strong detections of the low-velocity groups clearly visible at scale $J = 3$. The Arcturus and KFR08 streams appear stronger at the smaller Galactocentric radii. Based on the analysis of all stars in action space, the Arcturus stream is an elongated structure in L_z . These means it covers a wider range of orbits, unlike, for example, the Hercules stream.

5. The vertical extent of Arcturus and associated streams

We will focus on three low-velocity structures (g1, g2 and g9) detected in region 00 in action space between $V \approx -70$ to -160 km s^{-1} . The groups that we associate with these velocities in the solar region are the AF06, Arcturus, and KFR08 streams. The question is if they are related, are they elongations of each other, and how different they are compared to the Hercules stream? The Hercules stream is chosen as a reference as it is one of the most studied kinematic structures and is a relatively metal-rich disk structure with the dynamical origin with the Galactic bar (e.g. Bensby et al. 2007; Ramya et al. 2016; Pérez-Villegas et al. 2017). One of the main peaks of the Hercules stream is group g18 detected in action space. We study properties of this group for a comparison with the low-velocity structures.

To further distinguish the three streams we investigate how the number density of stars in the Hercules, Arcturus, AF06, and KFR08 streams vary with vertical distance from the Galactic plane. Candidate member stars of the three streams were selected from the stellar sample constructed as described in Sect. 2 using the characteristic velocities of the streams that found for region 00 (see Table A.2). From now on, it is assumed that kinematic groups are defined as stars on similar orbits. We assume that a star belongs to a group if its radial action and angular momentum falls into an ellipse around the centre of the group as shown in Fig. 3.

The plot on the left-hand side in Fig. 7 shows the variation of the normalised number of stars in g1, g2, g9 and g18 streams as defined in action space (see Fig. A.2) with module of the distance from the Galactic plane $|Z|$ for region 00. The Hercules stream is slightly more concentrated towards the Galactic plane compared to the three low-velocity structures. To check if this is valid in the regions outside the solar neighbourhood stars in regions 01, 11, 21 and 31 (see Fig. 2) that are members of groups g1, g2, g9 and g18 were selected. A star is defined as a member of a group if it has J_r and L_z values located within an ellipse around a group in action space as shown in Fig. 2. Since actions are conserved quantities along orbits of stars in static potentials it is expected that the structures will show up at the same positions in L_z and J_r . The right-hand side plot in Fig. 7 is the same as the one on the left, but for regions 01, 11, 21 and 31. The Hercules stream is strongly concentrated to the Galactic plane and gets rapidly weaker with distance from the plane. At distances above $|Z| \gtrsim 0.7 \text{ kpc}$ the density of Hercules stream stars has essentially dropped to zero. In comparison, the g1, g2 and g9 structures reach larger heights from the plane. The disappearance of the Hercules stream after about 0.7 kpc is consistent with the results from Antoja et al. (2012) that detected the Hercules stream at lower confidence level at higher Z . To further probe the origins of the detected kinematic structures and how they relate

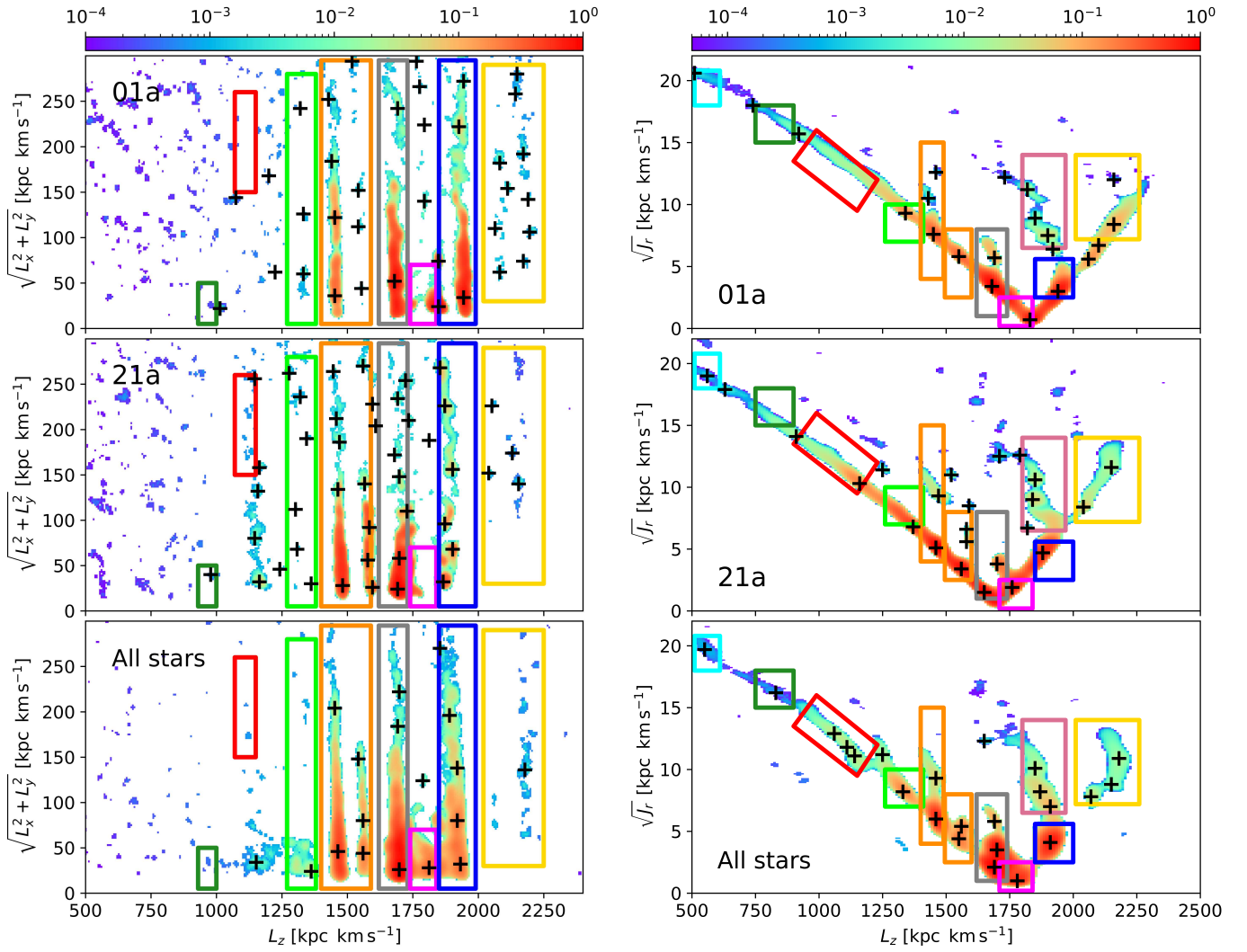


Fig. 6. Wavelet coefficient maps of regions 01a (top), 21a (middle) and all stars studied in this work (bottom) retrieved in $L_z - \sqrt{L_x^2 + L_y^2}$ (left column) and $L_z - \sqrt{J_R}$ (right column) space for scale $J = 2$. Colour bars show normalised wavelet coefficients. Black crosses show centres of the structures. Boxes around the crosses show location of kinematic structures based on the nearby sample 00 (see Figure 3). Colours of the boxes correspond to different names of the structures listed in the legend of Figure 3.

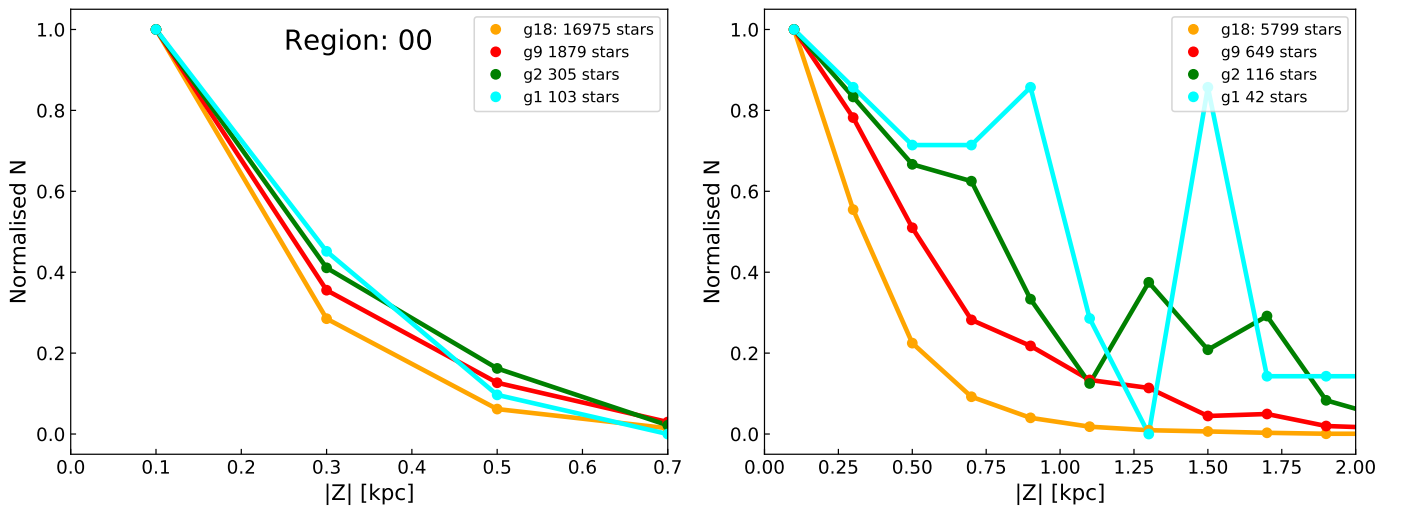


Fig. 7. A number of stars in Hercules, AF06, Arcturus and KFR08 versus module of distance from the Galactic disk $|Z|$ in region 00 (left) and in regions 01, 11, 21 and 31 (right).

Table 1. Median metallicities and corresponding dispersions of stars members of the groups located in the square defined by nine regions around the central region 00 that were selected from APOGEE and GALAH samples.

Group	GALAH		APOGEE	
	[Fe/H] _{median}	$\sigma_{[Fe/H]}$	[Fe/H] _{median}	$\sigma_{[Fe/H]}$
g18	0.0	0.2	0.0	0.2
g9	-0.2	0.3	-0.2	0.3
g2	-0.5	0.3	-0.5	0.2
g1	-0.6	0.3	-0.5	0.1

to each other we will make use of the detailed elemental abundance data from recent spectroscopic surveys.

6. Chemical properties of the kinematic streams

In this section we will investigate whether the detected streams show distinct elemental abundance patterns. To our aim the detailed abundance data from large spectroscopic surveys such as GALAH DR2 (Buder et al. 2018) and APOGEE DR 14 (Holtzman et al. 2018) were used. GALAH DR2 accounts over 340 000 stars and APOGEE DR14 accounts around 263 000 stars. Both GALAH and APOGEE have determined radial velocities for all their targets, and those stars does only to a very limited amount overlap with the subsample of stars in Gaia that comes with measured radial velocities in Gaia DR2. This means there will be just a few stars in each kinematic group when cross-matching GALAH and APOGEE with our sample that is constructed from the Gaia DR2.

Therefore, to increase the number of stars that can be associated with the streams that were detected and that have elemental abundances in the GALAH and APOGEE data releases, we compute space velocities U, V, W , angular momenta L_x, L_y, L_z and radial action J_r for all APOGEE and GALAH stars using astrometric data from Gaia DR2 and radial velocities from GALAH and APOGEE. Then the stars with $\sigma_U, \sigma_V \leq 20 \text{ km s}^{-1}$ and with good quality flags were select. For GALAH stars with good data quality flags were included: $flag_cannon = 0$ and $flag_x_fe = 0$, where where X is a chemical element, and for APOGEE the following quality flags were used: $X_FE_FLAG = 0$, where X is a chemical element. This left us a sample of 101 862 and 72 517 stars for the GALAH and APOGEE surveys, respectively. To select stars that are possible members of the detected kinematic streams we use our kinematic constraints for action space listed in Table A.2, meaning that a star must be within a specific range in L_z and J_r (fall into an ellipse around the structure as shown in Fig. 2).

Figure 8 shows the $X - Y$ distributions for the constructed GALAH and APOGEE samples. It is seen that APOGEE covers more stars of the Northern sky and GALAH covers mainly Southern part of the sky.

The top plots of Fig. 9 shows the $[\alpha/Fe] - [Fe/H]$ diagrams for stars in groups g1, g2, g9 and g18 selected in nine regions around the solar neighbourhood (01a_11a, 11a, 11a_21a, 01a, 00, 21a, 31a_01a, 31a and 21a_31a) for GALAH and APOGEE samples. We over-plot results for these nine regions simply because there are not enough stars in the low-velocity streams in each region to present them separately. The stars members of the groups were selected based on the properties of the groups in region 00 listed in Table A.2. Since actions are conserved quantities the groups are expected at the same positions after correcting

L_z values for the shift that arises due to difference in Galactocentric radii. The solid lines in these diagrams show the running mean for each stream. The shaded regions around each line show the corresponding 1σ dispersions around the mean value.

The bottom plots of Fig. 9 show generalised metallicity distributions for the same groups as in the upper plots. Median values of the metallicity distributions and corresponding dispersion of groups g18, g9, g2 and g1 are presented in Table 1 for the GALAH and APOGEE samples. The low-velocity streams generally have wide metallicity distributions and reaching lower metallicities down to $[Fe/H] \lesssim -1$. The Hercules stream is more metal-rich. These plots shows that the low-velocity streams could be high-alpha thick disk structures, while the Hercules stream is likely a mixture of both the thin and thick disks. Two-sided Kolmogorov-Smirnov tests are then used to check if the metallicity distribution of any of the streams come from the same distribution. In all cases the p -values were infinitesimally small, indicating that the null-hypothesis have to be rejected, meaning that all the distributions are different. Results using APOGEE and GALAH surveys are similar: the low-velocity streams appear to be thick disk structures, while the Hercules stream is a mixture of both the thin and the thick disks, and is a more metal-rich structure.

7. The origin of the Arcturus stream

In this section first we provide a brief overview of the debates around the origin of the Arcturus stream, then summarise the kinematic and chemical characteristics of the Arcturus stream from this work, and based on that we discuss possible origins of the stream.

7.1. Accretion origin: debris of a disrupted satellite

In Eggen (1996, 1998) it was shown that the Arcturus stream (then called a moving group) belongs to the old thick disk population. It was fitted with a 10 Gyr isochrone and the metallicity of Arcturus was estimated as $[Fe/H] \approx -0.6$. Similar properties were observed by Gilmore et al. (2002) and Wyse et al. (2006) who found a clump of stars at $V \approx -100 \text{ km s}^{-1}$ that were estimated to be about 10 – 12 Gyr old and metal-poor with $-2.5 < [Fe/H] < -0.5$. This is consistent with the properties of the Galactic thick disk.

One of the first attempts to explain the phenomenon of the Arcturus stream numerically was performed by Navarro et al. (2004). Assuming a merger event that happened 10 – 12 Gyr ago Navarro et al. (2004) obtained a structure with similar properties as the Arcturus stream. Navarro et al. (2004) also estimated the vertical component of the angular momentum of the group to be $L_z \approx 1000 \text{ kpc km s}^{-1}$.

Other evidence for a possible debris origin for the Arcturus stream comes from Helmi et al. (2006), who found that a satellite galaxy with similar orbital properties as the Arcturus stream can produce three kinematic over-densities. One of the groups was linked to the Arcturus stream and investigated further through a detailed elemental abundances analysis in Ženovieň et al. (2014). They found that the average metallicity of the stream is $[Fe/H] \approx -0.42$ and that its stars are about 8-12 Gyr old, which is consistent with the properties of the thick disk. Considering the results from Helmi et al. (2006), the Ženovieň et al. (2014) study supported the merger origin for the stream. On the other hand, a comparison with another detailed elemental abundance study by Ramya et al. (2012), who applied different selection

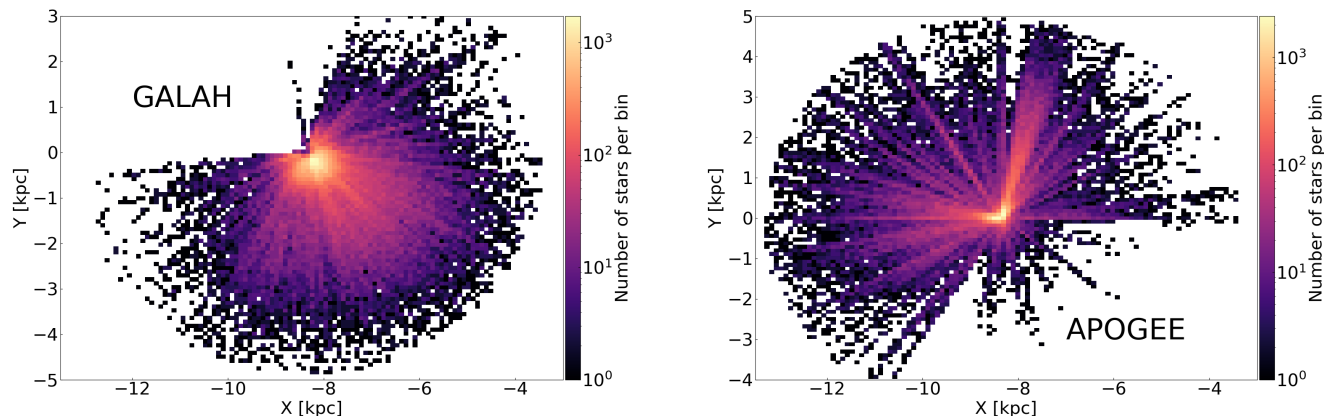


Fig. 8. $X - Y$ distributions for GALAH stars (left) and for APOGEE stars (right) with $\sigma_U, \sigma_V \leq 20 \text{ km s}^{-1}$ and good quality flags. The bin size is 0.1 kpc for both plots.

criteria for possible Arcturus stream stars, suggested that it is different from the thick disk and the two groups studied in these works are different.

An alternative approach to search for kinematic overdensities was proposed by Arifyanto & Fuchs (2006), and then followed by Klement et al. (2008) and Zhao et al. (2014). Using wavelet transforms they searched for clumps in plane defined by the $\sqrt{U^2 + 2V^2}$ and V space velocities, where U and V are radial and tangential velocity components, respectively. They detected many kinematic structures in the range $-200 \leq V \leq -80 \text{ km s}^{-1}$, including candidates for the Arcturus stream. Following the approach proposed by Helmi et al. (1999), Klement et al. (2008) and Zhao et al. (2014) studied angular momenta space defined by $\sqrt{L_x^2 + L_y^2}$ and L_z , the angular momenta components of the stars. They placed the Arcturus stream at $V \simeq -100 \text{ km s}^{-1}$ and $L_z \simeq 1000 \text{ kpc km s}^{-1}$. High eccentricity and low metallicity of the low-velocity streams lead to a conclusion that the Arcturus has a merger debris origin.

The above papers provide evidences that the Arcturus stream and other low-velocity streams can be explained as debris from disrupted satellite galaxies that merged with the Milky Way in the past.

7.2. Galactic origin: resonances

If debris origin for the observed streams is correct, the stars within a stream should have a distinct elemental abundance pattern different from what is observed for the Milky Way disk stars. A detailed chemical analysis of possible members of the Arcturus stream and another group called the AF06 stream, first assigned by Arifyanto & Fuchs (2006), was performed by Ramya et al. (2012). As no unique chemical features were found for either of the groups; their chemical compositions are similar to the background thick disk stars, being metal-poor, alpha-enriched, and have ages between 10-14 Gyr. This indicates that these structures are likely to have a dynamical origin within the Galaxy.

Another chemical analysis of the Arcturus stream was performed by Williams et al. (2009). The stellar sample was constructed based on results of the N-body simulations, where a satellite was accreted by the Milky Way. It was also here found that the stream stars are chemically inhomogeneous, being similar to the thick disk, and thus, cannot be called a moving group. The authors discuss a possible origin of the group within the

Milky Way, being dynamically formed due to Lindblad resonances. At the same time they do not reject the possibility of a merger origin.

Bensby et al. (2014) studied ages and chemical composition of the Galactic disk stars and briefly explored those that potentially could belong to the Arcturus stream ($-115 < V < -85 \text{ km s}^{-1}$). They found no chemical signature of a merger event, but rather that a dynamical origin is more probable due to similarities of chemical patterns of the group with the thick disk.

If the discussed spectroscopic studies question an accretion origin for the Arcturus, can the structure be reproduced in a resonant scenario via numerical simulations? Assuming resonances with the Galactic long bar, Gardner & Flynn (2010) simulated a kinematic group which has properties similar to the Arcturus stream. Numerical simulations performed by Monari et al. (2013) show similar result; the Galactic long bar can produce a feature that is consistent with the Arcturus stream.

All these findings lead to a discussion whether the Arcturus stream formed due to resonances or due to a merger event? Simulations assuming either of the hypotheses are able to reproduce a phase-space structure similar to the Arcturus stream. At the same time there is no clear consensus from the detailed elemental abundance studies.

7.3. Other hypothesis and recent findings

An alternative opinion on the origin of the Arcturus stream was proposed by Minchev et al. (2009). Assuming the existence of a dynamically unrelaxed population which formed after a merger event Minchev et al. (2009) simulated how the distribution of stars in the $U - V$ and $V - \sqrt{U^2 + 2V^2}$ changes with time. They found ring-like structures that represent a wave with streams appearing almost every 20 km s^{-1} in V , placing the Arcturus stream at -100 km s^{-1} . Based on the kinematics of the simulated structures the authors state that the Galactic disk was perturbed about 1.9 Gyr ago and match it with the time when the Galactic bar could have formed.

Another support of the ringing hypothesis came with the Gaia DR2 Gaia Collaboration et al. (2018a) release. The analysis of Gaia DR2 data revealed a rich arch- and ridge-like substructure in the phase-space that is a strong evidence that the Milky Way's disk is far from equilibrium and undergoes phase-mixing (Antoja et al. 2018; Ramos et al. 2018; Monari et al. 2018; Tian

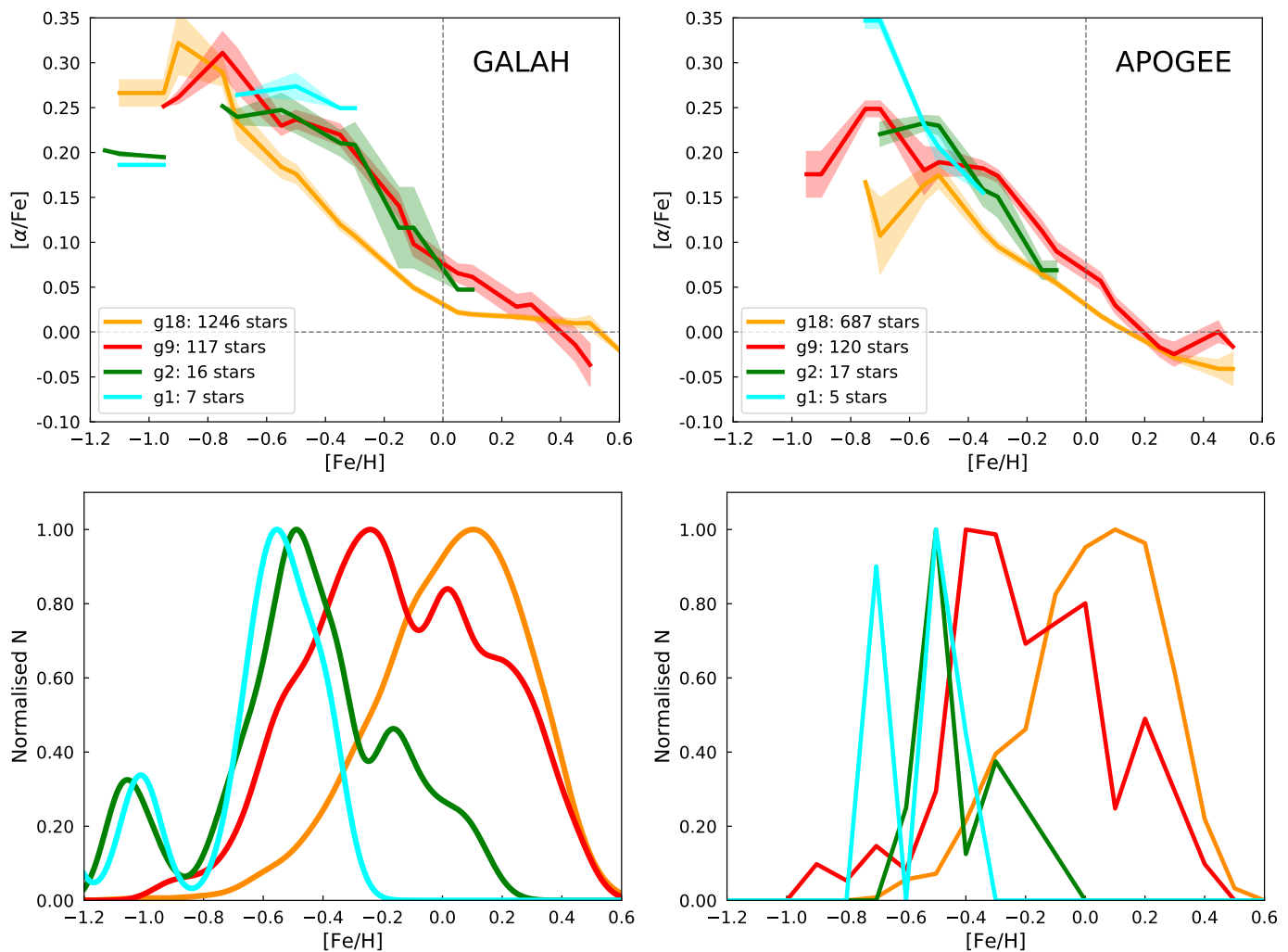


Fig. 9. *Top plots:* $[\text{Fe}/\text{H}] - [\alpha/\text{Fe}]$ trends for the streams selected from the GALAH and APOGEE data in action space in a square of nine regions defined by regions 01a_11a, 11a_21a, 21a_31a and 31a_01a. The solid lines show the running means of the $[\alpha/\text{Fe}]$ distributions in bins of $[\text{Fe}/\text{H}]$, and the shaded regions give the $1 - \sigma$ dispersions of the data around the means. The bin width when calculating running means is 0.05 dex. *Bottom plots:* Normalised generalised metallicity distributions for the stellar samples shown in the top plots. Here each star is represented by a Gaussian with central peak at the estimated metallicity and a width given by the uncertainty of the metallicity.

et al. 2018). This phase-mixing could be a result of external-perturbations due to a passage of the Sagittarius dwarf galaxy (e.g. Antoja et al. 2018). At the same time Hunt et al. (2018), Quillen et al. (2018) and Sellwood et al. (2019) show that the phase-space ridges could be a result of an impact of the Galactic spiral arms, but the simulations do not cover the low-velocity field. The Arcturus stream is one of the arch-like structures seen in Ramos et al. (2018), who performed a deeper study of the substructures with the wavelet analysis. If the Arcturus is a kinematic wave in the Galactic disk, then what triggers the formation of these structures, the bar, spiral arms or a merger event? What is the nature of Arcturus stream and how similar or different is it from the other kinematic structures?

7.4. The origin of the Arcturus stream in this study

Before discussing possibilities for the nature and origin of the Arcturus stream (g2) we summarise the properties of the kinematic substructures associated with the Arcturus stream that we so far have found:

- The rotational velocity of the Arcturus stream is $V \approx -127 \text{ km s}^{-1}$, and the vertical component of the angular momentum is $L_z \approx 840 \text{ kpc km s}^{-1}$. This is in agreement with the results from Navarro et al. (2004) who found the Arcturus stream at $V \approx -100 \text{ km s}^{-1}$ and $L_z \approx$ in the range between 700 and 1100 kpc km s^{-1} , Klement et al. (2008) who found it at $V \approx -120 \text{ km s}^{-1}$ and $L_z \approx 1000 \text{ kpc km s}^{-1}$, and Ramya et al. (2012) who found it at $V \approx -125 \text{ km s}^{-1}$ and $L_z \approx 811 \text{ kpc km s}^{-1}$.
- The Arcturus stream (g2), as well as the AF06 and KFR08 streams (g1 and g9) are detected not only in the Solar neighbourhood. The structures appear in a larger box defined by regions 01_12, 22_12, 22_32 and 02_32. The rest of the regions contain significantly less stars as well as distance uncertainties are larger (see Table A.1). That is why it is not possible to definitely answer if there are no kinematic structures in those regions, or if they are weaker, or if it is a consequence of the properties of the stellar sample.
- The Arcturus stream extends to about 2 kpc vertically from the Galactic plane. At the same time the Hercules stream stars appears to be disappearing at distances greater than $|Z| \gtrsim 1 \text{ kpc}$. The streams detected at even lower V veloci-

ties extend to even greater distances from the Galactic plane. This is consistent with the results from [Antoja et al. \(2012\)](#) who found that the Hercules stream has a lower detection level after $|Z| \gtrsim 0.6$ kpc.

- The Arcturus, KFR08, and AF06 streams are alpha-enhanced in the $[\alpha/\text{Fe}] - [\text{Fe}/\text{H}]$ diagram, and show similarities to the Galactic thick disk. They are clearly different from the Hercules stream which appears to be a mixture of the thin and thick disks. This is in agreement with, for example, [Bensby et al. \(2007\)](#); [Williams et al. \(2009\)](#); [Bensby et al. \(2014\)](#); [Ramya et al. \(2012\)](#).
- The Arcturus stream has a wide metallicity distribution spanning the interval $-1.2 \leq [\text{Fe}/\text{H}] \leq 0.2$ and peaking at ≈ -0.5 , which is not different from what has been found in other studies. [Eggen \(1996\)](#) found $[\text{Fe}/\text{H}] \approx -0.6$, and [Ramya et al. \(2012\)](#) found a more metal-poor range for the Arcturus stream, $-1.4 \leq [\text{Fe}/\text{H}] \leq -0.37$, peaking at $[\text{Fe}/\text{H}] \approx -0.7$.

Considering the chemical properties of the Arcturus stream (g2) we see that it is not a chemically homogeneous structure. This indicates that the Arcturus stream is not a moving group, similarly to what was found by [Williams et al. \(2009\)](#); [Ramya et al. \(2012\)](#); [Bensby et al. \(2014\)](#). Also, the metallicity distributions for the Arcturus, KFR08, and AF06 streams (g2, g1 and g9 respectively) are too wide for them to be called moving groups. At the same time, the mean metallicities are different for each stream, so, they appear to be independent structures, which is different from the conclusion by [Zhao et al. \(2014\)](#) that the Arcturus and AF06 streams should be regarded as one structure. It was also shown that a two-sided K-S tests rejected the hypothesis that any of the groups could come from the same population.

Groups g1, g2 and g9 found in this work appears to be, at least chemically, thick disk structures. Thus, we question the debris origin for the streams, in which case their chemical compositions should be different from the thick disk stars. This is different from the [Liu et al. \(2015\)](#) conclusion on a merger origin for the KFR08 stream. It is clearly seen that KFR08 has a wide metallicity distribution and its kinematics and chemistry are consistent with what is seen for the stars in the Galactic thick disk.

The two remaining possibilities for the origin of the Arcturus stream and the neighbouring KFR08 and AF06 streams (g2, g1 and g9 respectively) are the external-perturbation origin or being due to the resonances with the spiral arms or the Galactic bar. The results we have presented so far are consistent with the results from [Minchev et al. \(2009\)](#), who simulated the velocity distribution in the $V - \sqrt{U^2 + 2V^2}$ and $U - V$ planes assuming a merger event that perturbed the Galactic disk and caused an ongoing phase-mixing, inducing kinematic over-densities to be placed on the V axis every 20 km s^{-1} . This is essentially what we observe in this work. Arch-like structures are easily recognisable at Fig. 3 and similar to what was found in for example [Gaia Collaboration et al. \(2018b\)](#); [Antoja et al. \(2018\)](#) and [Ramos et al. \(2018\)](#). The patterns discussed in [Minchev et al. \(2009\)](#) are observed at the $V - \sqrt{U^2 + 2V^2}$ and action space, the arches observed in the $U - V$ plane become clumps. These clumps and arches are observed as lines in the angular momentum space. Within the uncertainties these features (arches, clumps and lines) show up $20\text{-}30 \text{ km s}^{-1}$ apart in the V velocity component. According to [Minchev et al. \(2009\)](#), this could be due to on-going mixing in the disk after a merger event. The fact that the low-velocity groups extend to higher $|Z|$ than the bar-originated structures inclines us to conclude on an external-

perturbation (phase-mixing) origin for the Arcturus stream and its neighbour KFR08 and AF06 streams is a possible scenario.

8. Summary

In order to resolve the nature of the Arcturus stream we analysed the velocity and angular momenta distributions of the *Gaia* DR2 stars at different Galactocentric radii. The analysis revealed the following:

- The analysis of four spaces defined by velocity, angular momenta and action components in 65 smaller volumes allowed to detect the previously well-studied Sirius, Pleiades, Hyades and Hercules streams; a few low-velocity structures that are associated with the AF06, Arcturus and KFR08 streams; many unknown clumps that might be a part of larger streams.
- The picture observed in the velocity space is consistent with the results from [Minchev et al. \(2009\)](#). Their model predicts kinematic structures to be placed every $20 - 30 \text{ km s}^{-1}$ in V . This is similar to what was observed with the *Gaia* DR2 sample: starting with the Sirius at 0 km s^{-1} and ending with the KFR08 stream at $\approx -160 \text{ km s}^{-1}$ we do observe kinematic structures every $V \approx 20 - 30 \text{ km s}^{-1}$ (taking into account velocity uncertainties and sizes of the structures).
- The arches observed in the $U - V$ plane are observed as clumps in the $V - \sqrt{U^2 + 2V^2}$ and action space and lines in the angular momentum space. [Minchev et al. \(2009\)](#) as well as [Antoja et al. \(2018\)](#) link these arches to the on-going phase-mixing in the Milky Way's disk due to a strong disk perturbation likely by a merger event.
- The low-velocity streams are observed further more from the disk at higher $|Z|$ compared to the Hercules stream which is currently considered as a structure caused by the Galactic bar (e.g. [Antoja et al. 2014](#); [Pérez-Villegas et al. 2017](#)). The KFR08 stream, which has the lowest values of V and L_z extends at least 2 kpc further from the Galactic disk, while the Hercules is located closer to the Galactic disk $|Z| < 0.7$ kpc.
- The majority of stars from the sample analysed in this work are within 1 kpc in $|Z|$ and according to ([Monari et al. 2013](#)) the Galactic bar can influence stellar motion up to $|Z| \approx 1$ kpc in the thin disk and up to $|Z| \approx 2$ kpc.
- The lower velocity groups are present mainly in the nearby regions. It is consistent with [Ramos et al. \(2018\)](#), where one of the discovered arches, that the authors associate with the Arcturus group, is located mainly in the Solar neighbourhood and within the Solar circle. At the same time this result can be a consequence of the fact that nearby regions contain more stars and distance uncertainties are smaller.
- [Ramos et al. \(2018\)](#) discuss the negative gradients of the rotational velocity of the structures with the Galactocentric radii. This gradient should be positive for the Cartesian velocities V . We do observe similar gradients in the $U - V$ plane.
- The analysis of the chemical abundances of stars that are members of the groups taken from the APOGEE and GALAH spectroscopic surveys confirmed that the AF06, Arcturus, and KFR08 resemble the thick disk chemical patterns. The groups cover wider metallicity ranges compared to the Hercules. The latest one appears to be a mixture of the thin and the thick disk stars, which is in agreement with the literature (e.g. [Bensby et al. 2014](#); [Ramya et al. 2016](#)). Estimated median metallicity of the Hercules in this work is $[\text{Fe}/\text{H}] \approx 0.0$, for example, [Ramya et al. \(2016\)](#) obtained $[\text{Fe}/\text{H}] \approx 0.15$.

- The two-sided K-S test performed for different combinations of the the groups (Hercules, AF06, Arcturus, KFR08) rejected the possibility for all of them to be drawn from the same distribution.

The the Arcturus, KFR08 and AF06 are kinematic structures that have rotational V velocities separated with a fixed step, that they extend farther from the Galactic plane compared to other over-densities such as the Hercules stream, and that they have chemical compositions consistent with the properties of the Galactic thick disk, points towards an origin for the structures related to the ongoing kinematic mixing or ringing in the disk, as was suggested in (Minchev et al. 2009). The recently discovered ridges and arches in the phase-space (Antoja et al. 2018; Ramos et al. 2018) with the *Gaia* DR2 including the Arcturus arch is another evidence that the low-velocity kinematic structures such as the Arcturus stream, could be a result of the external-perturbation process and were formed inside the Milky Way. But the question of origin of these phase-space warps is unresolved.

Though there has been done a lot of efforts to understand the nature of these phase-space waves with the *Gaia* DR2 data, we are still far from an unambiguous answer. Is it a merger origin as was originally proposed by (Minchev et al. 2009), or is it an influence of the spiral arms as suggested by, for example, Quillen et al. (2018); Hunt et al. (2018) and Sellwood et al. (2019)? Numerical simulations together with the chemical abundances from spectroscopic surveys like the *Gaia*-ESO survey (Gilmore et al. 2012), WEAVE (Dalton et al. 2014), and 4MOST (de Jong et al. 2019), in combination with upcoming *Gaia* data releases will broaden the opportunities for us to better understand the formation of the phase-space warps and might give a definite answer about the origin of kinematic structures like the Arcturus stream. Current observational evidence is however pointing towards a phase-space mixing origin.

Acknowledgements. We thank Prof. F. Murtagh for making available for us the MR software packages and Dr. P. J. McMillan for a valuable help when needed. T.B. was funded by the project grant "The New Milky Way" from the Knut and Alice Wallenberg foundation.

References

- Antoja, T., Figueras, F., Fernández, D., & Torra, J. 2008, *A&A*, 490, 135
 Antoja, T., Helmi, A., Bienayme, O., et al. 2012, *MNRAS*, 426, L1
 Antoja, T., Helmi, A., Dehnen, W., et al. 2014, *A&A*, 563, A60
 Antoja, T., Helmi, A., Romero-Gómez, M., et al. 2018, *Nature*, 561, 360
 Arenou, F., Luri, X., Babusiaux, C., et al. 2018, *A&A*, 616, A17
 Arifanto, M. I. & Fuchs, B. 2006, *A&A*, 449, 533
 Bailer-Jones, C. A. L. 2015, *Publications of the Astronomical Society of the Pacific*, 127, 994
 Bensby, T., Feltzing, S., & Oey, M. S. 2014, *A&A*, 562, A71
 Bensby, T., Oey, M. S., Feltzing, S., & Gustafsson, B. 2007, *ApJ*, 655, L89
 Bobylev, V. V. & Bajkova, A. T. 2016, *Astronomy Letters*, 42, 90
 Bovy, J. 2015, *The Astrophysical Journal Supplement Series*, 216, 29
 Bovy, J. 2016, *ApJ*, 817, 49
 Buder, S., Asplund, M., Duong, L., et al. 2018, *MNRAS*, 478, 4513
 Chakrabarty, D. 2007, *A&A*, 467, 145
 Dalton, G., Trager, S., Abrams, D. C., et al. 2014, in *SPIE Conf. Ser.*, Vol. 9147, 91470L
 de Jong, R. S., Agertz, O., Berbel, A. A., et al. 2019, *The Messenger*, 175, 3
 De Silva, G. M., Freeman, K. C., Bland-Hawthorn, J., Asplund, M., & Bessell, M. S. 2007, *AJ*, 133, 694
 Dehnen, W. 1998, *AJ*, 115, 2384
 Dehnen, W. 2000, *AJ*, 119, 800
 Dekker, E. 1976, *Phys. Rep.*, 24, 315
 Eggen, O. J. 1971, *PASP*, 83, 762
 Eggen, O. J. 1996, *AJ*, 112, 1595
 Eggen, O. J. 1998, *AJ*, 115, 2397
 Famaey, B., Jorissen, A., Luri, X., et al. 2005, *A&A*, 430, 165
 Feltzing, S. & Holmberg, J. 2000, *A&A*, 357, 153
 Gaia Collaboration, Brown, A. G. A., Vallenari, A., et al. 2018a, *A&A*, 616, A1
 Gaia Collaboration, Katz, D., Antoja, T., et al. 2018b, *A&A*, 616, A11
 Gardner, E. & Flynn, C. 2010, *MNRAS*, 405, 545
 Gilmore, G., Randich, S., Asplund, M., et al. 2012, *The Messenger*, 147, 25
 Gilmore, G., Wyse, R. F. G., & Norris, J. E. 2002, *ApJ*, 574, L39
 Helmi, A., Babusiaux, C., Koppelman, H. H., et al. 2018, *Nature*, 563, 85
 Helmi, A., Navarro, J. F., Nordström, B., et al. 2006, *MNRAS*, 365, 1309
 Helmi, A., Veljanoski, J., Breddels, M. A., Tian, H., & Sales, L. V. 2017, *A&A*, 598, A58
 Helmi, A., White, S. D. M., de Zeeuw, P. T., & Zhao, H. 1999, *Nature*, 402, 53
 Holtzman, J. A., Hasselquist, S., Shetrone, M., et al. 2018, *AJ*, 156, 125
 Hunt, J. A. S., Hong, J., Bovy, J., Kawata, D., & Grand, R. J. J. 2018, *MNRAS*, 481, 3794
 Johnson, D. R. H. & Soderblom, D. R. 1987, *AJ*, 93, 864
 Katz, D., Sartoretti, P., Cropper, M., et al. 2019, *A&A*, 622, A205
 Klement, R., Fuchs, B., & Rix, H.-W. 2008, *ApJ*, 685, 261
 Koppelman, H., Helmi, A., & Veljanoski, J. 2018, *ApJ*, 860, L11
 Kushniruk, I., Schirmer, T., & Bensby, T. 2017, *A&A*, 608, A73
 Lindegren, L. 2018, *Gaia Technical Note: GAIA-C3-TN-LU-LL-124-01*
 Liu, C., Feltzing, S., & Ruchti, G. 2015, *A&A*, 580, A111
 McMillan, P. J. 2018, *Research Notes of the American Astronomical Society*, 2, 51
 Minchev, I., Boily, C., Siebert, A., & Bienayme, O. 2010, *MNRAS*, 407, 2122
 Minchev, I., Nordhaus, J., & Quillen, A. C. 2007, *ApJ*, 664, L31
 Minchev, I., Quillen, A. C., Williams, M., et al. 2009, *MNRAS*, 396, L56
 Monari, G., Antoja, T., & Helmi, A. 2013, *ArXiv e-prints [arXiv:1306.2632]*
 Monari, G., Famaey, B., Minchev, I., et al. 2018, *Research Notes of the American Astronomical Society*, 2, 32
 Monari, G., Famaey, B., Siebert, A., et al. 2019, *arXiv e-prints*, arXiv:1908.01318
 Monari, G., Kawata, D., Hunt, J. A. S., & Famaey, B. 2017, *MNRAS*, 466, L113
 Navarro, J. F., Helmi, A., & Freeman, K. C. 2004, *ApJ*, 601, L43
 Pérez-Villegas, A., Portail, M., Wegg, C., & Gerhard, O. 2017, *ApJ*, 840, L2
 Quillen, A. C., Carrillo, I., Anders, F., et al. 2018, *MNRAS*, 480, 3132
 Ramos, P., Antoja, T., & Figueras, F. 2018, *A&A*, 619, A72
 Ramya, P., Reddy, B. E., & Lambert, D. L. 2012, *MNRAS*, 425, 3188
 Ramya, P., Reddy, B. E., Lambert, D. L., & Musthafa, M. M. 2016, *MNRAS*, 460, 1356
 Schönrich, R., Binney, J., & Dehnen, W. 2010, *MNRAS*, 403, 1829
 Sellwood, J. A. 2010, *MNRAS*, 409, 145
 Sellwood, J. A., Trick, W. H., Carlberg, R. G., Coronado, J., & Rix, H.-W. 2019, *MNRAS*, 484, 3154
 Skuljan, J., Hearnshaw, J. B., & Cottrell, P. L. 1999, *MNRAS*, 308, 731
 Starck, J.-L. & Murtagh, F. 2002, *Astronomical image and data analysis* (Berlin; New York: Springer), oCLC: 679368657
 Starck, J.-L., Murtagh, F. D., & Bijaoui, A. 1998, *Image Processing and Data Analysis*, 297
 Tian, H.-J., Liu, C., Wu, Y., Xiang, M.-S., & Zhang, Y. 2018, *ApJ*, 865, L19
 Trick, W. H., Coronado, J., & Rix, H.-W. 2019, *MNRAS*, 484, 3291
 Ženovienė, R., Tautvaišienė, G., Nordström, B., & Stokutė, E. 2014, *A&A*, 563, A53
 van der Walt, S., Schönberger, J. L., Nunez-Iglesias, J., et al. 2014, *PeerJ*, 2, e453
 Wegg, C., Gerhard, O., & Portail, M. 2015, *MNRAS*, 450, 4050
 Williams, M. E. K., Freeman, K. C., Helmi, A., & RAVE Collaboration. 2009, in *IAU Symposium*, Vol. 254, *The Galaxy Disk in Cosmological Context*, ed. J. Andersen, Nordström, B. M., & J. Bland-Hawthorn, 139–144
 Wyse, R. F. G., Gilmore, G., Norris, J. E., et al. 2006, *ApJ*, 639, L13
 Zhao, J. K., Zhao, G., Chen, Y. Q., et al. 2014, *ApJ*, 787, 31

Appendix A: Tables

Table A.1. The number of stars, median distance and median distance uncertainty for the stars located in the 65 regions (as defined in Fig. 1).

N	Region	N stars	D_{median} [pc]	$\sigma_{D_{median}}$ [pc]
1	00	666505	212	2
2	01	48759	851	45
3	02	13647	1689	181
4	03	6332	2483	386
5	04	3041	3285	677
6	05	1621	4083	932
7	11	70747	861	38
8	12	22070	1778	164
9	13	8991	2636	375
10	14	3521	3502	669
11	15	1685	4338	918
12	21	81838	777	38
13	22	24823	1602	171
14	23	10146	2392	410
15	24	3307	3204	803
16	25	1386	4011	1171
17	31	64875	868	38
18	32	19806	1778	164
19	33	10747	2624	365
20	34	4307	3489	655
21	35	1873	4329	826
22	22_11	18596	1798	209
23	22_12	13098	2258	306
24	22_13	8223	2853	495
25	22_14	4132	3522	724
26	22_15	2197	4216	898
27	22_31	27838	1780	194
28	22_32	18135	2242	284
29	22_33	9545	2839	458
30	22_34	5646	3507	690
31	22_35	2832	4200	922
32	02_11	11447	1942	215
33	02_12	8189	2546	349
34	02_13	3219	3321	608
35	02_14	2267	4145	852
36	02_15	308	4897	954
37	02_31	12179	1939	232
38	02_32	9594	2544	372
39	02_33	4786	3306	602
40	02_34	1887	4147	868
41	02_35	263	4881	903
42	12_01	13658	2042	217
43	12_03	4287	3177	589
44	12_04	1942	3893	847
45	12_05	1125	4605	1024
46	12_21	21401	1864	189
47	12_23	6129	2823	538
48	12_24	2440	3500	896
49	12_25	1195	4206	1173
50	32_01	13717	2044	219
51	32_03	3988	3176	609
52	32_04	2172	3871	829
53	32_05	1290	4592	1081
54	32_21	22441	1856	186
55	32_23	3331	3496	855
56	32_24	11387	2806	495
57	32_25	1447	4209	1166
58	01a	211846	453	12
59	11a	271059	444	10
60	21a	317397	387	9
61	31a	256489	448	10
62	01a_11a	127033	630	22
63	11a_21a	175045	568	18
64	21a_31a	184213	574	18
65	31a_01a	127733	636	22

Table A.2. Kinematic structures found in region 00 in the $U - V$ (Plane 1), $V - \sqrt{U^2 + 2V^2}$ (Plane 2), $L_z - \sqrt{L_x^2 + L_y^2}$ (Plane 3) and $L_z - \sqrt{J_r}$ (Plane 4) planes at scale $J = 2$. First column is a line number in the table; the second one denotes the plane; names of the groups as in Figure 3 are given in column 3 and names of the groups as in the literature are provided in column 4; number of stars in each group is given in column 5; median U , V velocities, median angular momentum L_z and median value of square root of radial action per group is given in columns 6-9; columns 8-13 are standard deviations of the same quantities as in columns 6-9.

N	Plane	Group	Name	N stars	U	V	L_z	$\sqrt{J_r}$	σ_U	σ_V	σ_{L_z}	$\sigma_{\sqrt{J_r}}$
					[km s ⁻¹]	[km s ⁻¹]	[kpc km s ⁻¹]	[kpc km s ⁻¹]	[km s ⁻¹]	[km s ⁻¹]	[kpc km s ⁻¹]	[kpc km s ⁻¹]
1	1	g1	A1/A2	173	39	37	2158	12	2	2	30	0.6
2	1	g2	γ Leo	2643	34	8	1926	7	2	2	28	0.5
3	1	g3	Sirius	6966	-13	6	1918	3.6	2	2	31	0.5
4	1	g4	Sirius	1659	-53	4	1900	6.3	2	2	30	0.5
5	1	g5	γ Leo	2277	47	3	1894	7.9	2	2	31	0.5
6	1	g6	Sirius	10303	12	2	1888	4.1	2	2	30	0.5
7	1	g7	Sirius	1416	-61	2	1887	6.9	2	2	30	0.5
8	1	g8	γ Leo	1080	65	1	1872	9.9	2	2	27	0.5
9	1	g9	Sirius	871	-79	0	1858	8.8	2	2	31	0.5
10	1	g10	γ Leo	785	73	-2	1844	10.6	2	2	28	0.5
11	1	g11	γ Leo	1881	57	-5	1819	8.5	2	2	32	0.5
12	1	g12	Coma Berenices	12046	-15	-7	1808	1.3	2	2	29	0.5
13	1	g13	Bobylev16	180	-118	-10	1776	13.1	2	2	31	0.5
14	1	g14	Coma Berenices	8439	8	-14	1745	2.4	2	2	30	0.5
15	1	g15	Pleiades/Hyades	960	-81	-14	1744	8.3	2	2	29	0.5
16	1	g16	Pleiades/Hyades	14380	-33	-16	1733	2.7	2	2	28	0.5
17	1	g17	Pleiades/Hyades	11749	-42	-19	1710	3.8	2	2	25	0.4
18	1	g18	Antoja12(12)	302	98	-21	1695	13	2	2	29	0.5
19	1	g19	Wolf 630	6104	21	-22	1678	4.1	2	2	29	0.5
20	1	g20	Dehnen98	4129	41	-25	1664	6.3	2	2	26	0.4
21	1	g21	Pleiades/Hyades	13084	-10	-25	1657	2.2	2	2	26	0.4
22	1	g22	Hercules	2604	-58	-37	1562	6.5	2	2	24	0.4
23	1	g23	Pleiades/Hyades	3428	25	-37	1561	5.7	2	2	27	0.4
24	1	g24	Hercules	1380	-82	-47	1473	9.5	2	2	27	0.4
25	1	g25	Hercules	3529	-15	-48	1468	5.8	2	2	25	0.4
26	1	g26	Hercules	4626	-37	-49	1463	6.6	2	2	22	0.4
27	1	g27	Hercules	2816	0	-50	1455	6.2	2	2	24	0.5
28	1	g28	Hercules	1593	-70	-51	1450	8.9	2	2	25	0.5
29	1	g29	Antoja12(15)	633	65	-52	1441	10.2	2	2	27	0.4
30	1	g30	HR1614	1286	9	-64	1342	8.2	2	2	25	0.5
31	1	g31	HR1614	1989	-16	-64	1343	8.1	2	2	25	0.4
32	1	g32	HR1614	1619	-26	-67	1321	8.5	2	2	24	0.5
33	1	g33	HR1614	1345	-36	-68	1313	8.9	2	2	25	0.5
34	1	g34	ϵ Ind	498	-83	-75	1252	12	2	2	25	0.4
35	1	g35	ϵ Ind	626	-73	-76	1247	11.5	2	2	24	0.5
36	1	g36	Arcturus	358	-13	-92	1118	11.6	2	2	23	0.6
37	2	g1	Arcturus	1840	-11	-91	1125	11.7	25	2	22	0.6
38	2	g2	AF06	2013	-12	-86	1168	11.1	26	2	24	0.7
39	2	g3	Hercules	1483	-85	-54	1431	10.4	57	2	26	0.8
40	2	g4	HR1614	7629	-10	-65	1337	8.3	20	1	23	0.5
41	2	g5	HR1614	8490	-9	-61	1366	7.8	19	1	24	0.5
42	2	g6	Hercules	14860	-10	-46	1482	5.8	19	2	27	0.5
43	2	g7	Sirius	2459	-60	1	1876	8	64	2	29	1.4
44	2	g8	Hercules	15404	-5	-40	1539	4.9	21	2	25	0.7
45	2	g9	A1/A2	1129	-5	38	2173	10.6	17	2	30	0.6
46	2	g10	Pleiades/Hyades	16788	-41	-19	1707	3.9	34	2	26	1.1
47	2	g11	γ Leo	4112	45	3	1893	7.4	49	2	31	1.3
48	2	g12	Pleiades/Hyades	38181	-7	-25	1660	2.5	14	2	27	0.7
49	2	g13	γ Leo	5460	30	7	1921	6.3	34	2	29	1.1
50	2	g14	A1/A2	3361	-5	22	2044	7	13	1	32	0.6
51	2	g15	Coma Berenices	26737	-2	-12	1766	1.2	10	2	29	1
52	2	g16	Sirius	19311	0	8	1926	4.3	9	2	27	0.5
53	2	g17	Sirius	19358	0	0	1872	2.9	5	2	31	0.5
54	3	g1	Pleiades/Hyades	81	-13	-23	1661	3.2	40	2	2	2.8
55	3	g2	Hercules	47	-12	-52	1439	6.6	47	2	2	2.3
56	3	g3	Hercules	66	-18	-41	1529	5.7	47	2	2	2.3
57	3	g4	Sirius	86	-6	4	1895	4.4	33	3	2	1.9
58	3	g5	HR1614	41	-17	-67	1325	8.7	45	2	1	1.9
59	3	g6	Pleiades/Hyades	171	-12	-20	1698	3.5	34	2	2	2.1
60	3	g7	Hercules	120	-27	-51	1452	6.7	34	2	2	1.3
61	3	g8	Sirius	165	-3	2	1890	4.2	35	3	2	2.2
62	3	g9	Pleiades/Hyades	264	-19	-20	1698	2.8	36	2	2	2.5
63	3	g10	AF06	17	-22	-94	1109	12.4	45	2	2	1.5
64	3	g11	A1/A2	41	-10	24	2064	8.1	38	3	2	2
65	3	g12	Sirius	263	-2	7	1926	4.6	29	3	2	1.7
66	3	g13	A1/A2	55	-13	26	2063	7.9	30	3	2	1.5
67	3	g14	HR1614	119	-11	-62	1350	8.4	38	2	2	1.3
68	3	g15	Hercules	359	-20	-39	1547	5.4	39	2	2	1.7
69	3	g16	Sirius	456	0	6	1914	4.3	28	3	2	1.7
70	3	g17	A1/A2	54	-16	24	2057	7.5	28	3	2	1.5
71	3	g18	HR1614	108	-17	-62	1349	8.4	39	2	2	1.6
72	3	g19	Hercules	379	-32	-48	1470	6.5	31	2	2	1.4
73	3	g20	Sirius	427	3	5	1919	4.2	23	3	2	1.5
74	3	g21	Arcturus	8	-44	-111	967	15.4	60	1	3	0.6
75	3	g22	Coma Berenices	644	-9	-7	1806	2	27	2	2	2.3
76	3	g23	Pleiades/Hyades	865	-21	-19	1703	2.5	25	2	2	1.7
77	3	g24	HR1614	90	-18	-61	1362	8.3	39	2	2	1.5
78	4	g1	KFR08	107	-13	-160	575	19.5	49	2	23	0.2
79	4	g2	Arcturus	303	-6	-127	841	16.1	40	3	23	0.2
80	4	g3	Antoja12(12)	122	103	-19	1707	15.1	125	3	22	0.3
81	4	g4	A1/A2	132	31	43	2223	13.3	42	4	22	0.2
82	4	g5	Hercules	326	-111	-50	1460	13	103	3	22	0.2
83	4	g6	A1/A2	255	27	30	2110	12.8	69	4	22	0.2
84	4	g7	Antoja12(12)	579	92	-19	1710	12.9	105	4	23	0.3
85	4	g8	γ Leo	405	84	-7	1805	12.7	102	4	22	0.2
86	4	g9	AF06	1836	-18	-92	1113	11.9	27	2	21	0.2
87	4	g10	γ Leo	803	77	-4	1828	11.4	84	4	23	0.3
88	4	g11	A1/A2	1026	-7	39	2177	10.9	26	3	20	0.3
89	4	g12	γ Leo	1765	64	0	1867	10	70	4	23	0.3
90	4	g13	Hercules	3649	-72	-50	1460	9.4	64	4	23	0.3
91	4	g14	γ Leo	3393	48	1	1878	8.3	57	4	24	0.2
92	4	g15	HR1614	8691	-15	-64	1342	8.3	22	2	21	0.3
93	4	g16	A1/A2	2922	-13	25	2064	7.7	20	3	20	0.3
94	4	g17	γ Leo	5271	33	6	1910	7	44	4	23	0.3
95	4	g18	Hercules	16701	-21	-49	1463	6.2	19	2	20	0.3
96	4	g19	Dehnen98	7245	36	-23	1679	6.1	47	4	22	0.3
97	4	g20	Pleiades/Hyades	15246	-15	-38	1551	4.6	19	3	22	0.3
98	4	g21	Sirius	22970	0	6	1916	4.1	15	3	22	0.3
99	4	g22	Pleiades/Hyades	21418	-39	-20	1699	3.9	29	4	22	0.3
100	4	g23	Pleiades/Hyades	32987	-13	-25	1664	2.4	11	3	22	0.2
101	4	g24	Coma Berenices	21624	-11	-11	1769	0.9	6	3	23	0.2

Table A.3. Kinematic structures found in region 00 in the $U - V$ (Plane 1), $V - \sqrt{U^2 + 2V^2}$ (Plane 2), $L_z - \sqrt{L_x^2 + L_y^2}$ (Plane 3) and $L_z - \sqrt{J_r}$ (Plane 4) planes at scale $J = 3$. First column is a line number in the table; the second one denotes the plane; names of the groups as in Figure 4 are given in column 3 and names of the groups as in the literature are provided in column 4; number of stars in each group is given in column 5; median U , V velocities, median angular momentum L_z and median value of square root of radial action per group is given in columns 6-9; columns 8-13 are standard deviations of the same quantities as in columns 6-9.

N	Plane	Group	Name	N stars	U [km s ⁻¹]	V [km s ⁻¹]	L_z [kpc km s ⁻¹]	$\sqrt{J_r}$ [kpc km s ⁻¹]	σ_U [km s ⁻¹]	σ_V [km s ⁻¹]	σ_{L_z} [kpc km s ⁻¹]	$\sigma_{\sqrt{J_r}}$ [kpc km s ⁻¹]
1	1	g1	A1/A2	44	-122	17	2003	15.9	2	2	34	0.5
2	1	g2	Sirius	10806	9	2	1890	3.9	2	2	30	0.5
3	1	g3	γ Leo	2325	49	0	1872	7.9	2	2	32	0.5
4	1	g4	Bobylev16	824	-83	-3	1840	9.1	2	2	30	0.5
5	1	g5	Coma Berenices	12027	-11	-6	1814	1.3	2	2	29	0.5
6	1	g6	Bobylev16	194	-118	-13	1750	12.9	2	2	29	0.4
7	1	g7	Pleiades/Hyades	14437	-33	-17	1726	2.7	2	2	28	0.5
8	1	g8	Antoja12(12)	332	96	-22	1686	12.8	2	2	30	0.5
9	1	g9	Pleiades/Hyades	14069	-14	-23	1672	2	2	2	28	0.4
10	1	g10	Wolf 630	5913	21	-24	1665	4.2	2	2	28	0.5
11	1	g11	Dehnen98	4086	41	-25	1659	6.4	2	2	26	0.5
12	1	g12	Hercules	4670	-37	-49	1463	6.5	2	2	22	0.4
13	1	g13	Hercules	1394	-81	-49	1464	9.6	2	2	25	0.4
14	1	g14	Hercules	2400	1	-53	1438	6.5	2	2	26	0.5
15	1	g15	HR1614	1769	-13	-66	1331	8.2	2	2	25	0.5
16	1	g16	ϵ Ind	544	-76	-77	1239	11.7	2	2	23	0.5
17	2	g1	Arcturus	1837	-13	-92	1113	11.9	28	2	22	0.7
18	2	g2	HR1614	7724	-14	-66	1330	8.5	24	2	24	0.5
19	2	g3	Hercules	15998	-20	-49	1463	6.3	24	2	25	0.5
20	2	g4	Hercules	15702	-12	-42	1524	5.4	25	2	29	0.7
21	2	g5	A1/A2	1270	-6	37	2167	10.5	21	2	32	0.6
22	2	g6	A1/A2	1835	-7	30	2108	8.8	17	2	36	0.6
23	2	g7	Pleiades/Hyades	40542	-11	-21	1696	2	17	2	29	0.9
24	2	g8	Sirius	21306	6	0	1865	3	10	2	33	0.8
25	3	g1	HR1614	35	-16	-68	1315	8.7	40	2	2	1.7
26	3	g2	Pleiades/Hyades	190	-11	-21	1692	3.3	39	2	2	2.6
27	3	g3	Hercules	125	-26	-50	1457	6.6	42	2	2	1.8
28	3	g4	Sirius	165	-3	2	1890	4.2	35	3	2	2.2
29	3	g5	HR1614	85	-33	-68	1308	9.2	37	2	2	1.5
30	3	g6	Sirius	522	6	4	1901	4.1	27	3	2	1.7
31	3	g7	Hercules	383	-31	-49	1464	6.6	33	2	2	1.4
32	3	g8	Pleiades/Hyades	939	-20	-20	1697	2.8	28	2	2	1.8
33	3	g9	Arcturus	8	-49	-106	1000	14.2	38	1	2	0.8
34	4	g1	KFR08	94	-14	-159	586	19.3	51	2	21	0.2
35	4	g2	Antoja12(12)	585	91	-18	1718	12.8	104	4	23	0.3
36	4	g3	A1/A2	1081	-6	38	2172	10.8	27	3	22	0.3
37	4	g4	Hercules	2939	-77	-49	1463	9.7	70	4	23	0.2
38	4	g5	γ Leo	3455	49	0	1869	8.3	58	4	24	0.2
39	4	g6	A1/A2	3076	-14	24	2058	7.6	21	3	21	0.3
40	4	g7	γ Leo	4959	35	6	1910	7.2	45	4	24	0.2
41	4	g8	Hercules	17305	-24	-49	1466	6.3	21	3	21	0.3
42	4	g9	Sirius	23880	0	5	1909	4	15	3	22	0.3
43	4	g10	Pleiades/Hyades	35424	-17	-22	1687	2.3	13	3	24	0.2